[AMERICAN JOURNAL OF SCIENCE, VOL. 278, SUMMER, 1978, P. 969-999]

THE CONDITIONS OF FORMATION OF THE KING ISLAND SCHEELITE CONTACT SKARN, KING ISLAND, TASMANIA, AUSTRALIA

TEUNIS A. P. KWAK

Department of Geology, La Trobe University,
Bundoora, 3083, Victoria, Australia

ABSTRACT. At the King Island Scheelite deposit (King Island, Tasmania, Australia) reactions between the chemically dissimilar calcic hornfels and marble have resulted in a zonation at their contact which ideally results in the development of green hornblende in the hornfels followed by a zone of green diopside–hedenbergite pyroxene, grossularite garnet, Fe–vesuvianite, wollastonite, and finally marble. Superimposed on and largely subsequent to this is the tungsten-bearing skarn in the still unaltered marble. The process involved a complex interaction between hornfels, marble, and a saline fluid to produce a nearly pure diopside–hedenbergite pyroxene rock of the hornfels with anomalous Mo and W values and the skarn. Intermediate between the marble and skarn either a (1) wollastonite–vesuvianite–scheelite rock or a (2) amphibole-rich skarn occurs, while between the hornfels and the pyroxene rock there is a hornblende-rich hornfels. Case (1) occurs where the volumetric hornfels/skarn ratio in the immediate area is large, whereas in case (2) it is relatively small.

The tungsten-bearing skarn consists of hedenbergitic pyroxenes with Mg relatively rich at the core which decreases to Mg-poor at the edge of the grains in both cases (1) and (2). The quantity of Mg present in the pyroxene very much depends on the volumetric hornfels/skarn ratio, the Mg being derived largely from the hornfels. Skarn garnets are zoned grossularite to andradite in case (1), whereas the reverse is true in case (2). This is due to Al being retained as grossularite garnet at the periphery of the skarns and released near the end of crystallization in case (2) but not case (1). In the case (2) skarns, fluid inclusion studies indicated homogenization temperatures, corrected for salinity and pressure (600 bars) of 350° ± 20°C at the core of garnet, 370° ± 20°C at two-thirds of the radius out, and 505° to 510° ± 20°C at the edge. Salinities at the core are low (≅5 wt percent equivalent NaCl), whereas at the 370° ± 20°C temperature they rise dramatically to nearly 30 wt percent NaCl or more which persists to the edge of the garnet. Tensional fractures, partly healed and filled with two-phase fluid, occur everywhere up to approximately the 370° ± 20°C temperature, where they terminate near a garnet growth layer containing minute wollastonite fibers. The phenomenon is interpreted to be due to faulting produced pressure-release causing the fluid to reach a two-phase area. Pyrrhotite in the skarn is always rimmed by pyrite suggesting, at their contact, a temperature of 310°C and a f_{S_2} of 10^{-10}. Scheelite often has a central powellite-rich core (~30 mol percent) which falls abruptly (to <1 mol percent) at a distance of half the radius of the crystals. Using pertinent thermodynamic data and the reactions involving (A) andradite–hedenbergite, (B) wollastonite–quartz–calcite, (C) powellite–scheelite–molybdenite–tungstenite, and finally (D) pyrite–pyrrhotite the following semi-quantitative values are suggested. The skarn began to form at T = 350° ± 20°C, $f_{O_2} < 10^{-42}$, $f_{CO_2} < 10^{-0.5}$, and $f_{S_2} < 10^{-10}$ from a relatively dilute solution. At the interpreted faulting period T = 370° ± 20°C, $f_{O_2} \cong 10^{-41}$, $f_{CO_2} \cong 10^{-0.5}$, and $f_{S_2} \cong 10^{-9.5}$ with the solution becoming fairly saline. Near the termination of the episode T = 505° to 510° ± 20°C, $f_{O_2} \cong 10^{-25}$, $f_{CO_2} \cong 10^{-1.2}$, and $f_{S_2} \cong 10^{-5.5}$. Pressure varied between 400 to 600 bars being initially high, low at the period of faulting (hydrostatic), and high again at the termination of the skarn producing episode. In skarns where the hornfels/marble ratio is low, the values of f_{S_2}, f_{H_2O}, and f_{CO_2} rose with falling f_{O_2} and temperature to produce a mixture of epidote, calcite, ferrohastingsite, quartz, and pyrite from the previously formed garnet skarn. This occurred near the skarn-marble interface.

INTRODUCTION

This paper deals with the conditions of formation of the King Island Scheelite deposit, Tasmania, as determined from mineralogical and fluid

inclusion studies. An accompanying study deals with the spacial relationships of different rock types present in the skarn as well as bulk chemical mass balance calculations (Kwak, 1978).

Skarn deposits of this type (andradite–hedenbergite–quartz–calcite ± sulphides ± Fe oxides ± scheelite) have been studied by a number of authors (Korobeynikov, 1968; Large, 1972; Brock, 1972; Morgan, 1975; Bartholomé and Dimanche, 1967; Scharbert, 1966; Edwards, Barker, and Callow, 1956). As pointed out by Mamontov (1968) and others, the deposits generally involve two main phases of skarn formation, namely, a scheelite producing phase and a concluding period where the previously formed minerals are altered to an epidote–ferrohastingsite–calcite–quartz ± molybdenite ± pyrite assemblage.

Accurate chemical data on coexisting skarn minerals are rare (Gustafson, 1974; Huchenholz and Yoder, 1971). Older data in which analysis was done on mineral concentrates are not of great use because of widespread internal chemical zoning, especially in such minerals as garnet. Analyses by Huchenholz and Yoder (1971), Brock (1972), and Morgan (1975) indicate that the garnet in skarns of this type are andradite–grossularite (mainly andradite) and pyroxenes, hedenbergite–johnsonite–diopside (mainly hedenbergite). These garnets often show a grossularite-rich core and a more andradite-rich outer rim (Morgan, 1975, p. 125; Brock, 1972, p. 3397), while the pyroxene zoning is largely unknown in these skarns. No data is known to me on the composition of coexisting scheelite, pyrrhotite, pyrite, and/or Fe oxides with garnet and pyroxene. Scheelites in contact skarn deposits are variable in composition but generally contain less than 20 mol percent $CaMoO_4$ with most samples containing less than 1 mol percent (Hsu and Gulli, 1973). Also, although crystal to crystal chemical inhomogeneity within samples is known (Morgan, 1975, p. 124), no coherent-model has been proposed to explain the phenomenon.

Fluid inclusion data on skarns are also rare, and no studies are known to me that closely integrate analytical mineral and fluid inclusion studies. Filling temperatures of inclusions in primary skarn minerals generally range from as low as 285°C (for hedenbergite, Kissling and Pomir Leanu, 1970) to 600°C (Korobeynikov, 1968). The salinities are not well known.

The purpose of this study is to integrate the textures, mineral compositions, and fluid inclusion data to produce a sequential model of events for the King Island scheelite deposit.

ANALYTICAL METHODS

Chemical compositions were determined by means of a Joel JXA-5A electron microprobe with computer control, located at the Department of Geology, University of Melbourne, using a beam current of 0.1 ma and an accelerating potential of 15 Kv. The following standards were used: SiO_2, wollastonite and quartz; Al_2O_3, corundum; TiO_2, rutile; Fe total and Ba, anandite; K_2O, potassium tantalite; Mn, Mn metal; Ni, Ni

metal, and Na, jadeite. The computer program for the reduction of electromicroprobe data was written by Mason, Frost, and Read (1969) with modifications by A. K. Ferguson. The analyses presented in most cases represent the average of three data points. Fluid inclusion data were determined using the heating and cooling stage facilities at the C.S.I.R.O. mineral chemistry laboratory, North Ryde, N.S.W. and the Chaixmeca stage in operation in this department.

MINERALOGY AND PETROLOGY

The geology of the deposit is well known (Nye and Knight, 1953; Edwards, Barker, and Callow, 1956) and will not be dealt with extensively here. Briefly, the two samples used in this study were collected within meters of each other and 123 m up dip from the granite contact. The mine series in which the skarn occurs consists of an interbedded thin hornfels and marble unit (banded footwall series) and other thicker hornfelsic and marble units. This dips 30° to 60° southwest toward the granite with little structural complication.

A. "Endoskarn".—Throughout the area of the open pit the thermal metamorphism due to the intrusion of the granodiorite has caused reaction between the chemically dissimilar hornfels and marble. In the ideal case, this has resulted in the following zonation: (A) marble, (B) hornfels, (C) amphibole hornfels, (D) pyroxene, (E) garnet, (F) vesuvianite, (G) wollastonite, (H) occasional scapolite and (I) marble (pl. 1). The individual zones are usually centimeters thick. The contact between (A) and (B) is gradational with the amphibole near-exponentially over a 2 cm distance until the amphibole constitutes essentially 100 percent of the rock at the amphibole hornfels–pyroxene contact. The pyroxene zone consists of a fine grained mosaic of green pyroxene with no amphibole. Bedding traces have been retained in the pyroxene but do not occur in the following garnet zone suggesting the rather abrupt pyroxene–garnet zone contact was once the hornfels–marble contact. The garnet near the pyroxene–garnet zone contact often forms stromatolite-like bodies convex away from the contact suggesting the garnet growth was initiated from a relatively few centers at the hornfels–marble contact. Minor pyroxene occurs in the garnet zone. The garnet–vesuvianite zone contact is again abrupt with both garnet and pyroxene persisting in the vesuvianite zone. Vesuvianite, pyroxene, garnet, and a small amount of calcite occur in the well-defined wollastonite zone.

The zonation (pl. 1) is only present in some places. In other parts of the sequence within meters of centimeters of the plate 1 locale and at an equal distance from the pluton, part of the zonation may be missing. If a very thin layer of what was once hornfels occurs in a volumetrically larger amount of marble, the hornfels may be entirely consumed leaving the zonation amphibole hornfels–pyroxene, garnet–vesuvianite–wollastonite. The ultimate products on complete reaction are the vesuvianite wollastonite and/or garnet zones. If a thin layer of what was originally marble occurs in a thick sequence of hornfels, the zones of vesuvianite

and wollastonite are often missing, and only the pyroxene and garnet ones are retained with the total loss of marble. In this and the previous case the reactions have proceeded until the reactants have been entirely consumed. The thicknesses of the zones vary greatly, the vesuvianite and wollastonite zones may be missing while hornfels still occurs. This case is believed to be due to incomplete reaction in response to low permeability in the hornfels, marble, or both.

The compositions of the minerals in the zonation are shown in appendix 1 and were measured from sample I (fig. 1). The fine grained bedded hornfels consists of plagioclase, brown biotite, pale green amphi-

PLATE 1

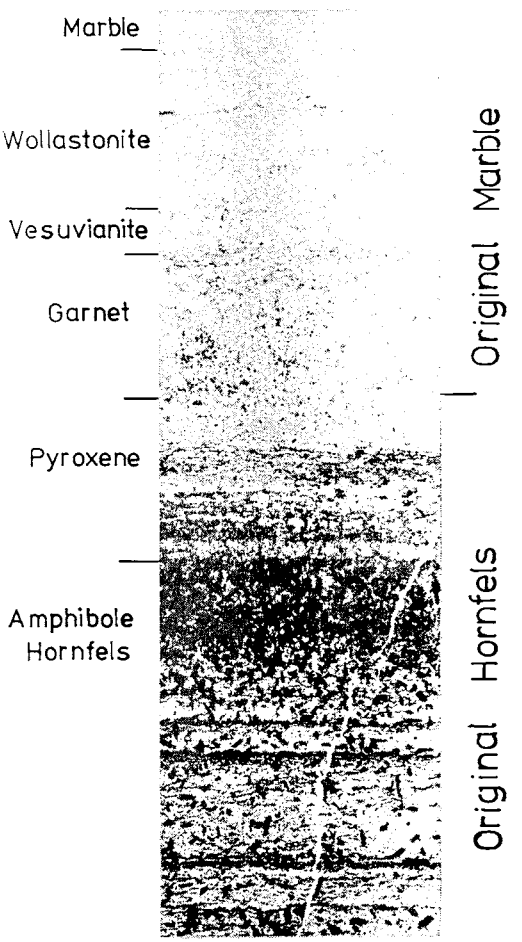

The ideal section showing the successive zones produced by reaction between hornfels and marble. Note the essentially exponential decrease of amphibole crystals away from the pyroxene–amphibole hornfels contact. The section is approx 1 cm long. The photo was taken using the thin section as a negative.

bole, sphene, quartz, zircon, green chlorite, pyrite, pyrrhotite, and chalcopyrite. The plagioclase (app 1, no. 28) is nearly pure albite (Ab = 98.4) with a small amount of K_2O (0.025 mol fraction) and some BaO (0.004). The biotite (app 1, no. 29) is annite$_{58.2}$ phlogopite$_{42.8}$ with Na greater than K (0.835 versus 0.649). The amphibole (app 1, no. 20) is tremolite-actinolite$_{85}$ hornblende$_{15}$. Sphene (app 1, no. 19) contains significant mole fractions of Fe (0.104) and Al (0.239) and may well contain OH as in inferred from its low total. The chlorite, which clearly is secondary in origin, was not analyzed but optically appears to be penninite. The amphibole in the amphibole hornfels (app 1, no. 21 and 22) is different from that in the hornfels proper as (A) the former consists of large dark green stubby crystals while the latter consists of pale green elongate crystals, (B) the amount of the amphibole in the amphibole hornfels is much greater than that in the hornfels, and (C) the former is approximately paragasite$_{40}$ hornblende$_{60}$ in composition, whereas the

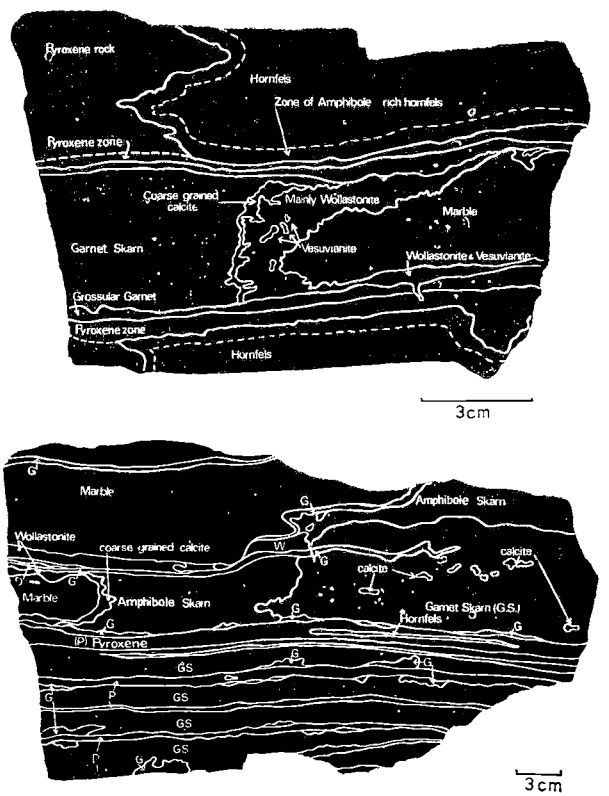

Fig. 1. Tracing from photos taken with ultraviolet light of the two specimens studied. The white specks in the garnet skarn, amphibole skarn, and wollastonite rock are scheelite.

G = garnet P = pyroxene GS = garnet skarn AS = amphibole skarn

latter is approximately $tremolite_{85}$ $hornblende_{15}$. Na appears to decrease toward the edge of the hornblende crystals (0.570 to 0.313 mol fraction). Within the amphibole hornfels and at its contact with the pyroxene zone, a continuous layer of pyrite exists.

The pyroxene zone is essentially a mozaic intergrowth of 100 percent $diopside_{71.5}$ $hedenbergite_{28.5}$ pyroxene (app 1, no. 11). The garnet zone consists of $grossularite_{57.5}$ $andradite_{42.5}$ garnet (app 1, no. 5) while vesuvianite (app 1, no. 27) is similar in composition to other contact metamorphic vesuvianite analyses (Deer, Howie, and Zussman, 1966, v. 1, p. 117, nos. 7 and 8) in having a significant Fe content (the Fe/Mg mol ratio is 0.47). While vesuvianite shows internal color zoning, only very minor variations in Ti, Fe, and Mg were analyzed. The pyroxene in the garnet zone and these two minerals in the vesuvianite zone are similar in composition to the respective analyses cited. The wollastonite in the wollastonite zone (app 1, no. 24) is very pure having only 0.009 mols of Fe and 0.006 mols of Mg. Again the minerals of the previous zone occur and are of a composition similar to the ones cited. The spacial relationships of the two skarn samples studied are shown in figure 2 and discussed in Kwak (1978); the analyses of constituent minerals are given in the appendix to this paper.

B. Sample I.—Sample I marble consists essentially of calcite with minor amounts of pyroxene, garnet, and an epidote mineral. The calcite (app 1, no. 17) is very pure ($Ca_{98.301}$ $Mg_{1.463}$ $Fe_{0.001}$ $Mn_{0.001}$). No dolomite was found using the electron microprobe, and the low MgO value of the calcite suggests none exists. The garnet (app 1, no. 4) is $grossularite_{30.2}$ $andradite_{24.0}$ $pyrope_{45.8}$ which is quite different from the garnet zone-garnets described. The epidote mineral was not analyzed but texturally appears to have formed at the expense of garnet and optically is epidote proper. Pyroxene is $diopside_{51.7}$ $hedenbergite_{42.0}$ $johannsenite_{6.3}$.

Sample I garnet skarn minerals are compositionally in sharp contrast to the ones so far described. The mineralogy is green pyroxene, brown garnet, scheelite, calcite, quartz, sphene, zircon, pyrite, pyrrhotite, pyrite, and molybdenite. The pyroxene (fig. 2; app 1, nos. 7 and 8) is primarily hedenbergite at the edge ($hedenbergite_{67.6}$ $diopside_{27.1}$ $johannsenite_{5.3}$) and diopside at the core ($hedenbergite_{31.1}$ $diopside_{65.0}$ $johannsenite_{3.9}$). The change in composition is very abrupt corresponding to distinct differences in the optical properties, such as birefringence. The hedenbergite–diopside contact is highly irregular (fig. 2) suggesting the diopside core was corroded prior to the hedenbergite crystallization. The core pyroxene is similar to that in the marble, and the former may well be a pre-exoskarn relict. The internal chemical variation in the skarn garnet is similar to the pyroxene in showing abrupt increases in Fe toward the edge (fig. 2; app 1, nos. 1 and 2), although the corresponding decrease is by Al_2O_3 and not MgO. The Fe is presumed to be mainly Fe_2O_3, because if Fe is calculated in this way, the totals best approach 100 wt percent. Like many of the King Island garnet skarns, the individual garnet crystals have a central unzoned core terminated by a layer

of minute fibrous crystals (which in sample II has been analyzed to be wollastonite) followed by a "growth-zoned" edge (pl. 2). At other localities than where sample I and II were collected, layers of wollastonite crystals occur in the outer growth-zoned edge of the garnets, and these occurrences are particularly common near known faults (Tan T. Hing, personal commun., 1976). The central core composition is approximately grossularite$_{34.5}$ andradite$_{66.5}$, while that at the edge is grossularite$_{14.4}$ andradite$_{85.6}$ (fig. 2 and app 1, nos. 1 and 2). The Mn increases toward the edge of the garnet (0.124 to 0.155 mols) while Ti decreases (0.53 to 0.29 mols). These values are different from those of the garnets found in the marble and show the core of the garnets in the garnet skarns are not relict. Small inclusions of pyroxene, quartz, calcite, sphene, and scheelite occur throughout the garnet crystals with the exception that quartz inclusions are not found near the wollastonite fibers already mentioned.

The scheelite (app 1, no. 18) contains only 4.7 mol percent powellite with few other impurities. The calcite (app 1, no. 14) has the composition $Ca_{98.828}$ $Mg_{0.005}$ $Mn_{0.342}$ $Fe_{0.782}$ which is in sharp contrast to the calcite in

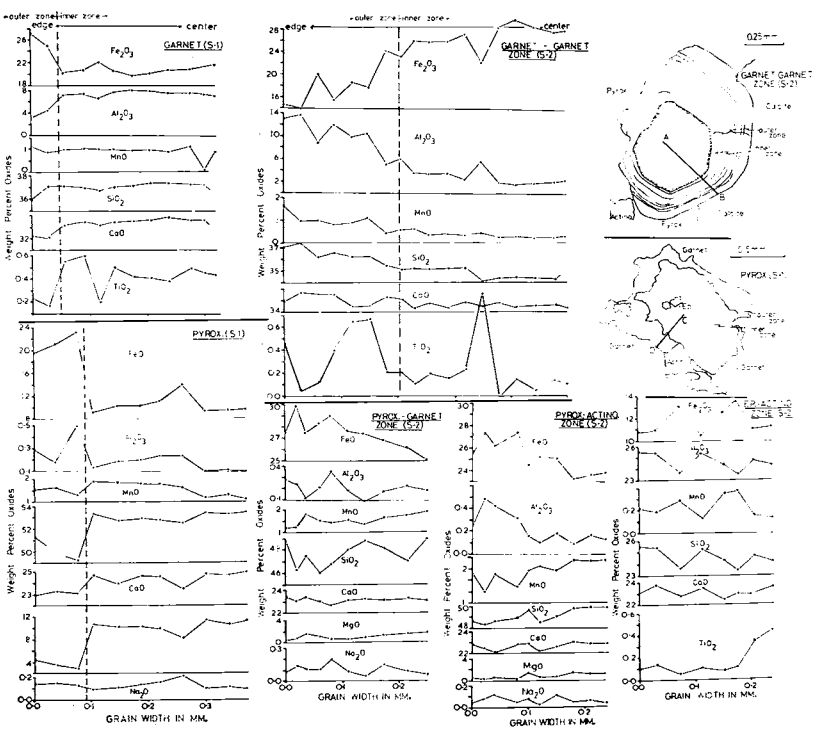

Fig. 2. Compositional variations across representative mineral grains from specimen I (S-1) and II (S-2). The term "garnet zone" and "actino zone" refer to the terms "garnet skarn" and "amphibole skarn" respectively in the text. The ordinates are in wt percent while the absissae are grain width in millimeters.

PLATE 2

Fluid inclusions in King Island skarn minerals

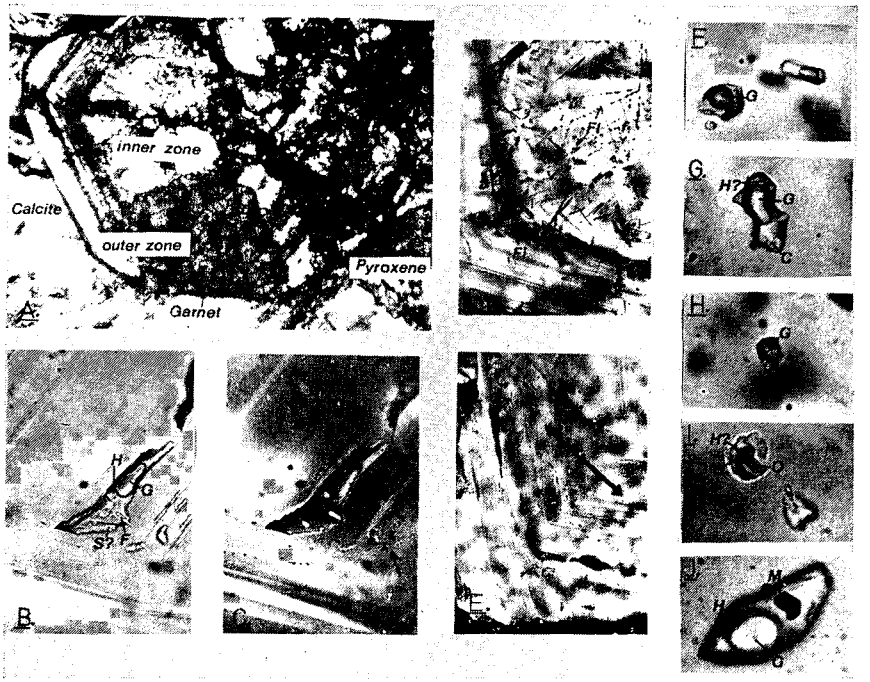

A. Large zoned garnet in specimen II garnet skarn, the chemical composition profile of which occurs in figure 1. Note the clear inner zone and layered outer zone. The garnet is anomalously birefringent and sector extinguishing (lower part of garnet) which is typical for andradite–grossularite garnets (~50X).

B. Multiphase primary fluid inclusion which has formed at the intersection of two growth layers. Garnet in specimen II garnet skarn. The daughter crystals are halite (H) with possible anhydrite (F) and sylvite (S). The inclusion gave a filling temperature of 450°C (125X).

C. The inclusion in (B) under polarized light showing the anisotropy of the tabular crystals (anhydrite?). The arrow shows a secondary train of fluid inclusions cutting the growth layers (125X).

D. The contact between the inner and outer zone of the garnet in (A) showing the fibrous wollastonite layer (Fi) at the contact and the randomly oriented fluid inclusion trails in the inner zone (25X).

E. The position of the fluid inclusion of (B) relative to the edge of the garnet. Note the fracture set (black line) which has been the loci for the formation of later secondary fluid inclusions.

F. Fluid inclusions within scheelite inclusions at the core of inner zone of a garnet in the same section as garnet (A). The inclusion gave a homogenization temperature of 330°C and an apparent salinity of about 5 wt percent equivalent NaCl (500X).

G. Fluid inclusion in vesuvianite from the wollastonite rock, specimen I. Note the halite (H) and mineral "C". This mineral was tentatively identified optically as a carbonate (500X).

H. Primary(?) fluid inclusion in specimen I pyroxene in unreacted marble. This possibly represents the country rock fluid, although the filling temperature would be very low (500X).

I. Primary(?) multiphase fluid inclusion in quartz in granite from nearest contact to the specimens. It contains little gas suggesting the fluid was undersaturated with respect to CO_2. H = halite, O = an olive colored, unknown, tabular mineral. It gave an apparent filling temperature of 160°C (500X).

J. A primary multiphase fluid inclusion in quartz from a quartz–scheelite–molybdenite (–feldspar) vein which cuts the previously formed garnet skarn approx 80 m from where specimens I and II were collected. The inclusion consists of gas (G), halite (H), and molybdenite (M). The latter is most likely an accidental crystal. Filling temperature = 330°C (200X).

the marble. The garnet skarn calcite has reequilibrated to the new chemical conditions. The garnet skarn pyrite (app 1, no. 30) is very pure having only 0.010 mols of Mn (versus 1.020 mols of Fe) as a minor contaminant. Small amounts of amphibole and epidote have formed at the expense of pyroxene and garnet respectively. These have not been analyzed using the electron microprobe, but optically they are similar to those in the sample II amphibole skarn (to be described later).

Between the garnet skarn and the wollastonite rock is a thin zone of coarse grained calcite (app 1, no. 15) which is intermediate in composition to the calcites in the marble and the garnet skarn ($Ca_{99.994}$ $Mg_{0.000}$ $Mn_{0.003}$ $Fe_{0.003}$). The wollastonite rock consists mainly of white wollastonite and brown vesuvianite with minor amounts of brownish garnet, pale green pyroxene, calcite, scheelite, pyrite, and rare molybdenite. The wollastonite (app 1, no. 23) is very pure having only 0.005 mols of calculated Fe^{+2} (versus 0.009 in the wollastonite of the wollastonite zone endoskarn mentioned) and significantly more Mn (0.010 in the wollastonite rock versus 0.002 in the endoskarn). The vesuvianite (app 1, nos. 25 and 26) is very uniform in composition and similar to the endoskarn vesuvianite (Fe/Mg = 0.49 for the former and 0.47 for the latter). The garnet (app 1, no. 2) is similar to that in the marble, but the pyroxene (app 1, no. 9) is diopside (hedenbergite$_{11.8}$ diopside$_{86.3}$ johannsenite$_{1.9}$). It is possible, however, that the modal abundance and Fe/Mg ratios of the pyroxenes in both the wollastonite rock and the marble are very dependent upon the composition of the particular interbed within the original limestone and that these varied. The pyroxene and garnet in the wollastonite rock are chemically much more similar to those in the marble than those in the garnet skarn described. The scheelite, molybdenite, and pyrite were not analyzed. The calcite is identical to this in the marble in FeO and MnO but lower in MgO (app 1, no. 16). The MgO decrease could, perhaps, explain the high MgO values in the pyroxene or the existence of the vesuvianite.

Spacially, the relation of the pyroxene rock to the hornfels is essentially the same as that of the garnet to the marble. Similarly, where the garnet skarn has an intermediate wollastonite rock between it and the marble, the pyroxene rock has an amphibolite hornfels between it and the hornfels proper. The pyroxene rock consists of greater than 98 percent pyroxene with very minor minute included grains most of which are quartz. The composition of the pyroxene is hedenbergite$_{43}$ diopside$_{50.6}$ johannsenite$_{6.4}$ which is intermediate in composition between the edge and the core pyroxene compositions in the garnet skarn pyroxene (app 1, nos. 7 and 8) in Fe and Mg but enriched in Mn. The Mg composition of the pyroxene is most likely related to the relative immobility of Mg as has been shown in the accompanying study (Kwak, 1978). The Na_2O values are also relatively high (0.5 percent jadeite) which is similar to the values in the garnet skarn. The pyroxene analysis near the pyroxene rock–garnet skarn contact (app 1, no. 12) is very similar to that well within the

pyroxene rock but quite different from that in the endoskarn pyroxene zone described in sample I. The spacial relations imply that the reactions producing the endoskarn zonation continued before, during, and after the exoskarn forming episode. The continuity of the garnet zone, dividing the garnet skarn zone from the pyroxene rock is clearly shown. Analysis 12 was taken where the corresponding pyroxene zone (endoskarn) should have extended; however, the pyroxene composition here (hendenbergite$_{42.0}$ diopside$_{51.7}$ johannsenite$_{6.3}$) is different from that in the pyroxene zone (hedenbergite$_{28.4}$ diopside$_{71.0}$ johannsenite$_{0.6}$). This shows the pyroxene zone-pyroxenes equilibrate in composition to the new exoskarn conditions. This is not true in the case of the garnet zone (endoskarn) and very different from that in the garnet skarn (app 1, nos. 1 and 2).

C. Exoskarn — sample II.—Sample II (fig. 1) is similar to sample I except that (A) an intermediate amphibole skarn exists between the marble and the garnet skarn instead of a wollastonite rock, and (B) the hornfels has been almost entirely consumed.

The garnet skarn contains a proportionally greater amount of calcite and pyroxene with a smaller amount of garnet to that in the sample I garnet skarn (for modal abundances, see Kwak, 1978). The degree of alteration of pyroxene and garnet by amphibole and epidote (+ calcite) is also greater. The chemical composition of garnet (fig. 2; app 1, nos. 31, 32, and 33) vary from andradite$_{43.2}$ grossularite$_{51.4}$ spessartite$_{5.4}$ at the edge to andradite$_{89.6}$ grossularite$_{9.1}$ spessartite$_{1.3}$ at the core. The zoning here is thus inverse to that in sample I. The inverse relationship of Mn to the interpreted Fe^{+3} may be due to a different valence state of Mn or simply that it varies directly with Fe^{+2} which increases toward the edge. The latter case cannot be resolved with the instruments at hand.

The pyrope component of these garnets is negligible ($\cong$0.3 percent). The internal physical features of sample II garnets are similar to sample I garnets in there being a clear core, a layer of fibrous wollastonite in the garnet, and an outer complexly color-zoned area. The wollastonite fibers (app 1, analysis 49) have the composition wollastonite$_{98.2}$ hedenbergite$_{1.4}$ johannsenite$_{0.4}$ which is well within the range of wollastonite compositions. The fibers are very small in diameter, 20 to 30 mμ (see pl. 2-D), making it possible the electronmicroprobe beam was not entirely on the wollastonite but partly on the garnet as well. This possibility can be ruled out, because the Al values in the wollastonite are very low (0.012), while those in the accompanying garnet are relatively high (0.800 mols). Small inclusions of quartz, scheelite, and pyroxene occur throughout the garnet crystals in sample II with the exception that quartz does not occur where the wollastonite does, as in sample I.

The coexisting pyroxene is similar to that in sample I showing a gradual zonation from hedenbergite$_{82.8}$ diopside$_{11.0}$ johannsenite$_{6.2}$ at the core to hedenbergite$_{92.3}$ diopside$_{3.3}$ johannsenite$_{4.3}$ at the edge (app 1, nos. 35 and 36; also fig. 2). The lower MgO is probably related to the fact that volumetrically there is less hornfels present in sample II than

in sample I. The accompanying study has shown that nearly all the Mg is hornfels-derived. Occasionally growth zones are observed within crystals, but nothing as abrupt as in the sample I pyroxenes was observed. The scheelite in the garnet skarn is most commonly chemically zoned (pl. 3) with a powellite rich core (for example, 29.8 mol percent) dropping off abruptly to nearly pure scheelite at the edge (0.3 mol percent powellite). Other impurities are very minor in amount (app 1, nos. 43 and 44). Calcite in the garnet skarn is similar to the sample garnet skarn (app 1, no. 42). In addition, sample II garnet skarn contains sphene, zircon, quartz, pyrite, pyrrhotite with amphibole, and epidote

PLATE 3

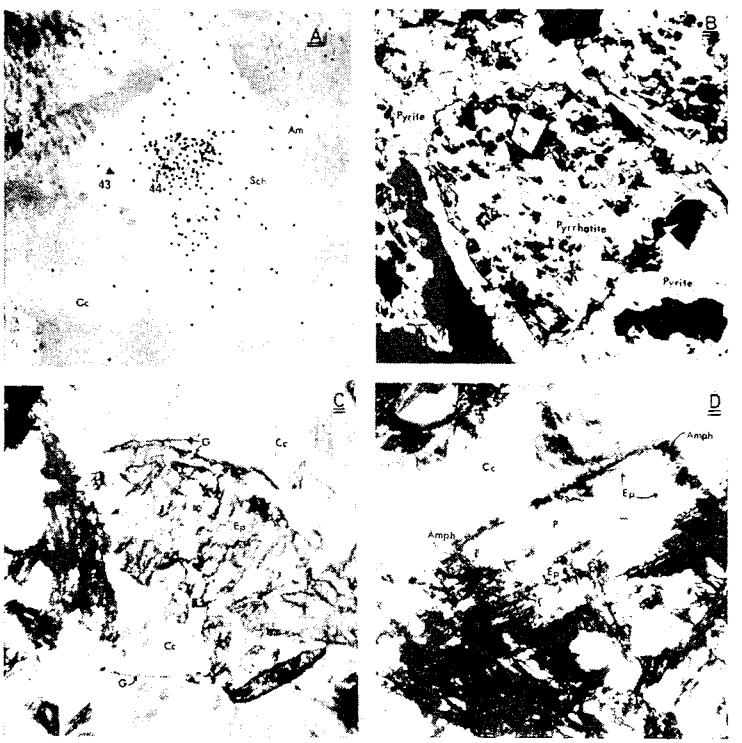

Textures used to justify the use of various reactions in the garnet skarn.

A. A scheelite crystal showing a molybdenum-rich core and molybdenum-poor edge. The photo is taken with total backscatter (electron microprobe) with a Mo radiation photo superimposed. Numbers 42 and 43 refer to analyses in appendix I. The grain is approx 100 microns wide.

B. A pyrite rim around pyrrhotite in reflected light suggesting the increase of f_{S_2} near the end of the skarn forming episode. The pyrrhotite is approx 500 microns wide.

C. A garnet pseudomorph retaining a garnet rim but internally having been replaced by calcite + epidote. The pseudomorph is approx 300 microns in its longest dimension.

D. Hedenbergite partly replaced and rimmed by ferrohastingsite and epidote. The grain is approx 300 microns in its longest dimension.

Cc = calcite Sch = scheelite Ep = epidote G = garnet P = pyroxene

forming at the expense of pyroxene and garnet respectively. The molybdenite is generally in and near the powellite-poor scheelite, never in the powellite-rich scheelite. The pyrite occurs as single grains and as a rim around pyrrhotite.

The amphibole skarn is an altered garnet skarn, where the garnet is almost entirely reacted to epidote + calcite ± pyrite (pl. 3) and the pyroxene to amphibole ± quartz as has been shown in the bulk chemical analysis study (Kwak, 1978). The textures are identical to those shown by Morgan (1975, p. 128). The garnet relicts are variable in composition, and, because it is a later alteration rather than related to the main skarn forming episode, one would expect the relicts to be grossular-rich, andradite-poor. In some cases, this has not been found to be true, where analyses were essentially of andradite (app 1, no. 34) with very little grossularite. The reason for this is unknown except that these could represent an adradite-rich zone developed during the growth of the garnet which somehow has persisted. The garnet commonly forms an atoll texture with the center being mainly calcite ± epidote. The pyroxene generally has been less altered than the garnet.

The pyroxene composition and internal chemical zoning (app 1, nos. 37 and 38; fig. 1) is very similar to that in the garnet skarn. The mineral alters to amphibole ± quartz ± Fe sulphides. The yellow-green epidote in the amphibole skarn forms both as irregular masses pseudomorphic after garnet or as large zoned crystals. The large crystals have light and darker green growth zones which show significant differences in birefringence; however, no systematic change in bulk chemistry was observed (app 1, nos. 45 and 46; fig. 1) related to these differences. TiO_2 increases from 0.006 to 0.013 mols toward the center of the grains, while other elements are highly variable. The epidote group mineral has the composition of epidote proper.

The amphibole forms long fibrous crystals with diamond-shaped cross sections. It is found as an alteration product of pyroxene (pl. 3-D) but not garnet. In composition (app 1, no. 47) it is close to the composition of hornblende (using Deer, Howie and Zussman, 1966, p. 1681), and it is distinct from the tremolite and hornblende present in the amphibole hornfels. Pyrite forms a rim about pyrrhotite as it does in the garnet skarn (pl. 3). The compositions of the two minerals (app 1, nos. 50 and 51) are relatively pure, Mn and Cu being only minor impurities. The formula for the pyrrhotite is approximately $Fe_{0.95}S$ at the pyrite–pyrrhotite interface. Calcite (app 1, no. 40) having the general composition $Ca_{97.9}\ Fe_{0.8}\ Mn_{1.3}\ Mg_{0.0}$ is higher in Mn to that in the garnet skarn (Mn = 0.8) but lower in Fe (Fe = 1.1). In contrast, the epidote appears to contain less Mn than the garnet it replaces (0.18 versus 0.23 wt percent) and the amphibole much less Mn than the pyroxene it replaces (0.86 versus 1.53 wt percent). The excess Mn so released could account for the slight increase of Mn in the calcite and would suggest the calcite has reequilibrated to the new conditions that produced the amphibole.

The calcite in the coarse grained calcite layer intermediate between the marble and the amphibole skarn (app 1, no. 41) has the composition $Ca_{99.42}$ $Fe_{0.29}$ $Mn_{0.29}$ $Mg_{0.10}$. This composition is intermediate between that in the marble ($Ca_{99.90}$ $Fe_{0.10}$) and in the amphibole skarn. In addition, the marble contains grossular garnet and diopsidic pyroxene very similar in composition and form to that found in sample I marble.

FLUID INCLUSION DATA

The fluid inclusion data were determined using the equipment at the C.S.I.R.O. laboratories at North Ryde (New South Wales) and with Chaixmeca gear at La Trobe University. The assumptions and extrapolations using fluid inclusion data are many, particularly when dealing with very saline fluids as discussed by Roedder (1967). In the present study, temperatures were corrected for salinity extrapolating from the results of Sourirajan and Kennedy (1962). The precision of the temperature data is probably in the range of ±20°C, although the possible error may well be less.

A homogenization pressure of 0.6 kb was assumed, partly on stratigraphic evidence and partly on the basis of chemical evidence to be discussed below. All the skarn minerals contain fluid inclusions of various types; however, because of the excellent optical and chemical zoning present in the garnets and also, the mineral's known refractory nature, it has received the most attention. The main problem with using garnet fluid inclusions is the mineral's high refractive index and the subsequent contact effects at edge of the fluid inclusion. These sections had to be ground thin and polished on both sides. As mineral inclusions of scheelite, quartz, and pyroxene occur throughout, the garnet is coexisted with these minerals during the entire history of the skarn formation, thus making it ideal for monitoring conditions during the process. All garnets in the garnet skarn have a clear central "inner zone" (pl. 2-A) and distinctive color zoned outer zone. Usable fluid inclusions are uncommon enough in a single garnet crystal, so that the inclusions in different garnets were analyzed relating each to the common internal features. The inner zone invariably contains trains of two-phase fluid inclusions which are randomly oriented and undoubtedly represent fluid-filled, partly healed, fractures. The lack of any distinct orientation of the trains suggests the fracturing occurred due to circumferential tension. A mechanically isotropic material such as garnet can be expected to fail in this way due to a sudden increase in temperature or decrease in pressure. These fractures extend to the inner zone-outer zone boundary, where they stop near a concentric layer of garnet containing numerous minute fibrous wollastonite crystals (pl. 2-D).

Evidence for the primary (that is, co-crystallization fluid) nature of fluid inclusions in the inner zone is difficult to find, because of the lack of color (growth) zoning, but this is much easier to show in the outer zone. Plate 2-F shows multiphase inclusions aligned parallel to the intersection of two such series of color zones related to the garnet morphology.

Cutting across the color zoning are trains of two phase inclusions which were undoubtedly formed in fractures caused by shear failure which occurred after the garnet had ceased growing. These now partly healed fractures do extend beyond the edge of the garnet and partly across coexisting pyroxene in some places.

Primary inclusions in the core of the garnets are rare, but fluid inclusions in scheelite mineral inclusions are more common. Plate 2-F shows such inclusions in sample II garnet skarn. An average homogenization temperature of 330°C was found with an apparent salinity of approx 5 wt percent equivalent NaCl. The salinity measurement is tentative because of the small size of the fluid inclusions, but the low value is consistent with the observation that no "primary-appearing" fluid inclusions in the garnet inner zones contained NaCl crystals. Fluid inclusions in the outer zone of the garnet but near the inner-outer zone contact yielded average homogenization temperature of 338°C with high salinities (≅30 wt percent equivalent NaCl).

The multiphase fluid inclusions pictured in plate 2-A, -B, and -C yielded average homogenization temperatures of 450°C, while ones slightly farther from the garnet edge slightly lower 443°C. Both consisted of a liquid phase, gas, halite, possibly anhydrite, and possibly sylvite. The anhydrite identification is on the basis of the apparently strong birefringence, moderate to strong relief, tabular crystal form, and the existence of two cleavages approximately at right angles. This does not exclude other materials such as $FeCl_2 \cdot 2H_2O$ or $Fe_2(SO_4)_3 \cdot 6H_2O$ (leusenite), although it is questionable if the solution could be concentrated enough to precipitate these. The primary inclusions occurring near the garnet edge contain approx 30 to 35 wt percent NaCl. Primary fluid inclusions in pyroxene, quartz, and scheelite coexisting with the garnet were rare. Correcting for salinity, the probable temperatures during garnet crystallization were 350° ± 20°C at the cores, 370° ± 20°C where the wollastonite fibers occur, and 510° ± 20°C near the edge while 505° ± 20°C closest to the edge.

Fluid inclusions in garnets in sample I garnet skarn had homogenization temperature of near 328°C at their cores often with the high birefringent mineral (anhydrite?) but no observed NaCl. No measurable fluid inclusions were found in the rims which is, in part, due to the much finer grain size of the garnet in that specimen. In both the skarns, secondary fluid inclusions homogenized in the range 150° to 180°C.

That the wollastonite rock in sample I formed associated with the primary fluid found in the garnet skarn is supported not only by the occurrence of scheelite in the latter rock type but also by the high salinities of the inclusions in wollastonite and vesuvianite (pl. 2-G). Liquid, gas, halite, and a high birefringent mineral tentatively identified as a carbonate but possibly anhydrite occur. The high salinities suggest the fluids are primary in origin. These fluid inclusions are distinctly different from those found within the accompanying marble in sample I in that

the latter rock type contains scarce diopsidic pyroxene containing randomly scattered, cubic fluid inclusions (pl. 2-H). The primary nature of the latter fluid inclusions is inconclusive but may well represent the original country-rock fluid.

Two phase gas-liquid fluid inclusions in calcite and actinolite in the sample II amphibole skarn gave homogenization temperatures near 184° and 210° respectively, although it could not be proved conclusively that these are primary. The temperatures are near those occurring as definite secondary origin in the garnets in the garnet skarn.

The skarns locally contain quartz–scheelite–molybdenite–feldspar veins which have formed normal to the layering in the skarns. These usually contain numerous multi-phase fluid inclusions in both the scheelite and quartz. Plate 2-J shows an inclusion containing liquid, gas halite, and a hexagonal platey, metallic mineral that is almost certainly molybdenite. Assuming the molybdenite is fairly thick, no data exist that would suggest this molybdenite can be concentrated to a high enough amount in such a saline fluid to precipitate the large crystal observed, and it must be concluded the molybdenite is not a daughter crystal but rather represents a crystal accidently included. These molybdenite crystals are, however, relatively common in the quartz fluid inclusions. The average homogenization temperature was 330°C, whereas freezing point was at +4.2°C suggesting a phase such as $CO_2 \cdot 5\frac{3}{4}\ H_2O$ was present (see Roedder, 1963). No positively identified immiscible CO_2 fluid was observed in any of the fluid inclusions at any temperature in this study.

THE CONDITIONS OF FORMATION OF THE SKARN

The conditions under which the skarn formed can be calculated, if (A) reactions can be written based on either textural data (pl. 3) or if both the mineral products and the reactants of a writable reaction are present in the skarn and (B) pertinent thermochemical data are available. Much data of the calcium silicates found in skarns at 25°C and 1 kb are available, but to determine the conditions at the elevated temperatures and pressures indicated by the fluid inclusion data, extrapolations must be made. As a consequence, it must be understood that the following results are only semiquantitative.

To do the calculations, it is necessary to suggest first a model for the skarn producing process on the basis of the mineralogical, chemical, and fluid inclusion data presented. The justification for some of the statements will be discussed in the last section. The process began at 360° ± 30° at a pressure of 400 to 600 bars producing andradite garnet, hedenbergite pyroxene, powellite-rich scheelite, pyrrhotite, quartz, calcite, and sphene. These conditions persisted until the garnets attained roughly two-thirds their final diameters after which a sudden release of CO_2 pressure occurred. This was perhaps due to overpressure caused by increasing P_{CO_2} evolved from the calc–silicate producing reactions and the subsequent pressure release of a CO_2 rich fluid phase due to faulting. The result was the tensional failure by fracturing

of the garnet with the deposition of a thin concentric layer of garnet containing fibrous wollastonite. No quartz inclusions occur in the garnet at this level, the decreased CO_2 pressure now favoring the stability of wollastonite over quartz + calcite. The garnet composition changes gradually from this point with many perturbations to a more grossular composition at the edge of sample II. Here sample II garnet data are used mainly because from a volumetric point of view, this sample best represents the major part of the deposit. The pyrrhotite composition at the pyrrhotite–pyrite contact of the sulphide bodies described suggests a temperature near 310°C and an f_{S_2} of near 10^{-01} bars, which is near the 360° ± 30°C described above. The abrupt change from powellite-rich scheelite to powellite-poor scheelite + molybdenite probably refers to this event. Pyroxene is less changeable but generally tends toward a more hedenbergite rich, johannsenite-poor, and diopside-poor composition.

The variability of composition mentioned could be due to periodic pressure release and/or a greater mixing of fluids from the newly formed fracture zones. Increased f_{S_2} produces (A) pyrite in preference to pyrrhotite, (B) molybdenite + near pure scheelite to powellite-rich scheelite, and (C) indirectly, grossular to andradite.

As a greater and greater proportion of the marble becomes skarn the permeability decreases and the circulation of fluids become more and more restricted. Crystal growth decreases, although temperatures rise to near 510° ± 20°C. A slight drop of temperature occurs at the edge of the garnet to about 505° ± 20°C just before crystallization of the primary scheelite skarn is terminated.

Continuously, reaction between the hornfels and the marble during the entire period persists, however, when permeabilities for the skarn producing fluid drop due to the completion of crystallization of the scheelite skarn assemblage, P_{CO_2}, P_{H_2O}, P_{S_2}, a_{K^+}, and a_{Na^+} increase locally in the still relatively permeable and fine grained marble. These are a product of the hornfels–marble reactions and react with the skarn to alter it to a mixture of amphibole, epidote, quartz, calcite, and pyrite. Conditions may have been as low as 150°C, and the fluid was again relatively dilute.

The combination of the mineral analyses with the fluid inclusion data and relevant thermochemical and experimental data allow the calculation of large numbers of possible reactions. Unfortunately, thermochemical data on the behavior of species such as Al^{+++}, Fe^{++} Fe^{+++}, and Mg^{++} at elevated pressure and temperature are unknown, so that only a model for the evolution of the skarn in f_{S_2}, f_{O_2}, f_{CO_2}, T, and total P space has been attempted.

The following relations were used

$$\underset{\text{andradite}}{Ca_3Fe_2Si_3O_{12}} + CO_2 + \underset{\text{quartz}}{SiO_2} \rightleftarrows \underset{\text{hedenbergite}}{2CaFeSi_2O_6} + \underset{\text{calcite}}{CaCO_3} + 1/2\,O_2 \qquad (1)$$

$$\underset{\text{scheelite}}{CaWO_4} + S_2 + CO_2 \rightleftarrows \underset{\text{tungstenite}}{WS_2} + \underset{\text{calcite}}{CaCO_3} + 3/2\ O_2 \quad (2)$$

$$\underset{\text{powellite}}{CaMoO_4} + S_2 + CO_2 \rightleftarrows \underset{\text{molybdenite}}{MoS_2} + \underset{\text{calcite}}{CaCO_3} + 3/2\ O_2 \quad (3)$$

$$\underset{\text{calcite}}{CaCO_3} + \underset{\text{quartz}}{SiO_2} \rightleftarrows \underset{\text{wollastonite}}{CaSiO_3} + CO_2 \quad (4)$$

$$\underset{\text{pyrrhotite}}{FeS} + 1/2\ S_2 \rightleftarrows \underset{\text{pyrite}}{FeS_2} \quad (5)$$

The data to allow the calculations of eq (1) were derived from Schearer (ms), Gustafson (1974), Robie and Waldbaum (1967), and Kennedy (1954). Schearer's andradite enthalpy data (of formation from the oxides) at 965°K was extrapolated to 573, 673, 773, and 873°K by use of the ΔCp data of Kelly (1960). The calculation assumed that ΔCp is constant over the temperature interval considered. ΔS data, necessary for the free energy calculation, were approximated by subtracting the ΔS of Al_2O_3 from the ΔS of grossularite (in Robie and Waldbaum, 1967) and adding the ΔS of Fe_2O_3. Entropy values for andradite at 1000°C are given by Schearer as 201.6 cal/deg from his data, 214.43 from the sum of the entropies ($\Sigma S°_{oxides}$) of the constituent oxides, and 205.95 by Fyfe's approximation. Similarly the values for grossularite are 182.0, 197.07, and 183.40. The entropies of Al_2O_3 and Fe_2O_3 at 1000°C (as in Robie and Waldbaum) are 60.44 and 43.08 respectively. Taking Schearer's, the $\Sigma S°_{oxides}$, and Fyfe's approximation values the differences of entropy between grossularite and andradite are 19.60, 17.36, and 22.55 cal/deg respectively. These compare very well with the entropy difference between entropies of Al_2O_3 and Fe_2O_3 of 17.36 and make the approximation quite reasonable. The ΔCp variations of Al_2O_3 and Fe_2O_3 over the interval 573 to 873 (Kelley, 1960) are essentially linear.

Free energy data for hedenbergite were calculated using Gustafson's experimental results for the reaction

$$3CaFe_2Si_3O_{12} + 9SiO_2 + Fe_3O_4 \rightleftarrows 9CaFeSi_2O_6 + 2O_2$$

The previously derived $\Delta G_{andradite}$ plus thermochemical data for the other species from Robie and Waldbaum were used to give free energy values of −602.48, −586.23, −569.18, and −552.22 kcal for the temperatures above. These again compare favorably when considering known ΔG values for the comparable pyroxene, diopside. ΔG values for CO_2 were determined using Kennedy's (1954) P–V–T data, calculating the compressibility factor α and graphically intergrating the values in α–P space for different values of temperature to determine fugacities and finally ΔG values at total pressures of 300, 600, 900, and 1200 bars. These pressure intervals and values were used because the fluid inclusion data imply varying pressure values during crystallization within this interval.

The values for reaction (1) at different total pressures and temperatures in log f_{O_2}-log f_{CO_2} and log f_{O_2}-log f_{S_2} space are shown in figure 3. The curves would move to lower log f_{O_2} values by perhaps half a log unit, if the free energy data for CO_2 is too low by the value Burnham and Wall's (personal commun.) data suggest. The effect of having solid solutions of andradite and hedenbergite with grossularite and diopside respectively would also move the curves to lower log f_{O_2} values by a fraction of a log unit assuming the solid solutions behave ideally. Considering the assumptions used, the figure must, however, clearly be viewed semi-quantitatively.

For reactions (2) and (3), the free energy values for $CaWO_4$, $CaMoO_4$, WS_2, and MoS_2 were determined by extrapolating Robie and Waldbaum's data to higher temperatures assuming ΔCp = constant and $V\Delta P = 0$ for the solid phases. The previously determined ΔG_{CO_2} values were used. The plot of this reaction on the log f_{CO_2}-log f_{O_2} (fig. 3) was done using, for reference, the fugacity sulphur values on the pyrite–pyrrhotite curve of Toulmin and Barton (1964) at the appropriate values of temperature. It must be borne in mind that this is, strictly speaking, not valid, as conditions near the end of the primary crystallization of the skarn were in the pyrite field. Ideal mixing of $CaWO_4$ and $CaMoO_4$ is assumed in the diagrams.

The ΔG values for the solid phases in reaction (4) were mainly derived from Robie and Waldbaum (1967), while the CO_2 values were those previously discussed. The values at the pressures calculated were very close to related ones determined by Greenwood (1967) at 1 and 2 kb. The NaCl content of the fluid, however, greatly decreases the possible CO_2 content of an aqueous solution (Takenouchi and Kennedy, 1965). The effect of this would be to increase the stability of wollastonite and move the points in figure 3 up perhaps by as much as a log unit for the salinities mentioned in this study.

The data for reaction (5) were taken from Toulmin and Barton (1964). It must be borne in mind that the total pressure for the experiments from which the data were determined is low, although the authors believe the pressure effect is small. If mineralogical and chemical changes mentioned were to occur, namely the powellite-rich to the powellite-poor scheelites, andradite-rich to grossular garnet and pyrrhotite to pyrite zonation change during crystallization of the deposit, curves for eq (1), (2), (3), (4), and (5) should cross at the same point. These should relate to an approximate temperature of 370° ± 20°C and a pressure of 400 to 600 bars. The pyrrhotite composition gives a temperature near 310°C with an accompanying f_{S_2} of 10^{-10}. It is equally most reasonable to propose that the powellite-rich scheelite assemblage gave way to a powellite-poor scheelite + molybdenite assemblage, when the f_{S_2} was sufficiently high to form pyrite in preference to pyrrhotite. However, it would be extremely fortuitous, if these curves were to cross at the same point considering the assumptions made in the calculations. Points A,

B, and C in figure 3 show the two values where curves related to eqs (1) + (4), (2 + 3) + 4, and 1 + (2 + 3) cross. The most reliable curves in the author's estimation are those not involving the sulphur species and the scheelite because of the greater assumptions in both the calculations and the original experimental work, thus, the intersection points of curves 1 and 4 are taken with the clear implication that conditions were near the wollastonite–quartz + calcite boundary.

The measured solid solution of garnet and hedenbergite would move curves 1 back up to half a log unit. Assuming larger values for f_{CO_2} as suggested by Burnham and Wall's data would also shift the curves 1 to lower f_{O_2} values and curves 4 to higher f_{CO_2} values. The shift of curves 1 would be to bring point C up closer to A and B. The fact that the three points do occur in close proximity to each other supports the view that the zonations observed occurred more-or-less at the same time.

In the amphibole skarn of sample H garnet and hedenbergite breakdown in two or all of the following ways

$$\underset{\text{hedenbergite}}{\tfrac{1}{2}Na^+ + \tfrac{1}{2}K^+ + 5Ca(FeMg)Si_2O_6} + 4CO_2 + H_2O \rightleftarrows \underset{\text{amphibole}}{(NaK)Ca(MgFe)_5Si_8O_{22}(OH)_2} + \underset{\text{quartz}}{2SiO_2} + \underset{\text{calcite}}{4CaCO_3} \quad (6)$$

or

$$\underset{\text{hedenbergite}}{\tfrac{1}{4}Na^+ + \tfrac{1}{2}K^+ + 6Ca(FeMg)Si_2O_6} + S_2 + 5CO_2 + H_2O \rightleftarrows \underset{\text{amphibole}}{(NaK)Ca(MgFe)_5Si_8O_{22}(OH)_2} + FeS_2 + \underset{\text{calcite}}{5CaCO_3} + \underset{\text{quartz}}{4SiO_2} \quad (7)$$

and

$$\underset{\text{garnet}}{3Ca(AlFe)_2Si_4O_{12}} + CO_2 + H_2O + O_2 \rightleftarrows \underset{\text{epidote}}{2Ca(AlFe)_3Si_3O_{12}(OH)} + \underset{\text{quartz}}{6SiO_2} + \underset{\text{calcite}}{CaCO_3} \quad (8)$$

or

$$\underset{\text{garnet}}{4Ca(AlFe)_2Si_4O_{12}} + CO_2 + S_2 + H_2O \rightleftarrows \underset{\text{epidote}}{2Ca(AlFe)_3Si_3O_{21}(OH)} + \underset{\text{pyrite}}{FeS_2} + \underset{\text{calcite}}{2CaCO_3} + \underset{\text{quartz}}{10SiO_2} + \tfrac{1}{2}O_2 \quad (9)$$

Stability relations were not determined for these reactions because of the lack of reliable thermochemical or experimental data for the amphibole (ferro-hastingsite–ferro-tschermakite) and epidote under the conditions present.

DISCUSSION

The general model proposed for the sequence of events by which the King Island scheelite deposit was formed is as follows

1. Deposition in late Precambrian-early Cambrian times of basal sandstone and siltstone followed by basic volcanics and interbedded limestone and calcic shale with a final basic volcanism.

2. Tilting of the sequence in the area of the deposit to the southwest at dips of 40° to 60°.

3. Intrusion of a Devonian hornblende-bearing granodiorite with accompanying aplitic and pegmatitic phases at a fairly high level in the crust (1-2 km depth).

4. At already relatively low temperatures (150°C?) recrystallization of the stratigraphic sequence occurred yielding marble with varying amounts of diopside pyroxene and grossularite garnet from limestone and hornfels from the calcic shale. The hornfels consists of albite, quartz, tremolite, biotite, epidote, chlorite, pyrite, chalcopyrite, sphene, and zircon. In addition, these two chemically dissimilar rock types reacted at their mutual borders. Going from the hornfels to the marble the products are (A) growth of hornblende in the hornfels, (B) an abrupt contact after which a diopsidic pyroxene zone occurs, (C) a successive grossularite garnet zone, (D) a vesuvianite zone, (E) wollastonite zone, and (F) locally scapolite zone. The zonation developed to varying degrees of completion depending upon permeability and bulk rock composition to produce in extreme cases grossularite + diopside, if a thin marble bed in a volumetrically greater amount of hornfels is entirely consumed, or vesuvianite + wollastonite and/or grossularite garnet, if a thin hornfelsic bed is entirely consumed. The process is viewed as having been initiated before, during, and after the skarn producing episode, until temperatures returned to the 150° to 200°C level after the solidification of the granodiorite. This temperature is reasonable when one considers that calculations of Helgeson (1969) show both grossular and diopside are possible phases at 25°C. The kinetics at these conditions may create a difficulty for the phases to crystallize, but this is not seen as a problem at 150° to 200°C.

5. At 350° ± 20°C the skarn producing process begins with the crystallization of an assemblage consisting of andradite garnet, hedenbergite pyroxene, powellite-rich scheelite, pyrrhotite, sphene, quartz, and calcite. The accompanying fluid is relatively dilute, salinities are near 5 wt percent equivalent NaCl, $f_{S_2} \leq 10^{-10}$, $f_{O_2} \leq 10^{-42}$, and $f_{CO_2} \leq 10^{-0.5}$.

6. Because of the calc–silicate producing reactions during the skarn production, large amounts of CO_2 are liberated keeping f_{CO_2} values within the quartz + calcite and not the wollastonite field. The loss of CO_2 by way of the interconnected passages from which the fluid came is important (Shoji, 1975). It is suggested in the present model that permeability in the skarn decreased in a similar fashion to the decrease of permeability with time due to crystallization in drilled hydrothermal sys-

tems (A. S. Ellis, personal commun., 1973). The C_2 over-pressure developed which eventually reached values greater than the rock cover could withstand, and these fractures released the CO_2. Faults of both pre-, syn-, and post-skarn origin occur in the mine. The pressure release changed the confining pressure of the system from lithologic ± CO_2 over-pressure to simply hydrostatic. These fractures may well have opened periodically to allow the loss of CO_2 pressure. The temperatures were near 370° ± 20°C, and the P–T conditions of the hydrothermal fluid reached a two phase area, releasing relatively large amounts of the volatile CO_2 and H_2O.

The area over which a vapor + liquid field existed may for a time not have extended to the surface, as this would have involved the loss of large amounts of heat. Possibly a vapor pocket existed which may or may not have extended to the surface, thus, a supercritical fluid could have occurred nearest the granodiorite, followed by a vapor pocket, and finally, a sub-critical fluid. The supercritical fluid becomes relatively more saline (25-30 wt percent NaCl), as more and more fluid is circulated through the system. This is either directly to the surface, if the two phase area extends to the surface terminating in a fumerole or by CO_2 and H_2O being transferred to the subcritical fluid by way of the vapor pocket terminating in hot springs. The sudden release of the CO_2 pressure caused the circumferential tensional fractures in the garnet, and because the CO_2 pressure is now relatively low, the assemblage quartz + calcite is unstable relative to wollastonite. After this event f_{S_2} increases so that pyrite is stable relative to pyrrhotite and powellite-poor scheelite + molybdenite relative to powellite-rich scheelite. The garnet shows greater variability in composition and color zoning after the suggested pressure-release event with a general tendency for Al to increase over Fe. This could be due to the increased salinity facilitating greater Al solubility or to mixing with fluids from other environments. The permeability has decreased, and it is possible a greater proportion of the skarn chemistry is derived from interchange with the hornfels as the accompanying study suggests. The following conditions prevailed during pressure-release event $f_{S_2} \cong 10^{-9.5}$, $f_{O_2} \cong 10^{-41}$, and $f_{CO_2} \cong 10^{-0.5}$ with total pressure near 400 to 600 bars (fig. 3).

7. The crystallization of the skarn continued. Reaction between the fluids, hornfels, and marble produced the skarn and the pyroxene rock. As the process proceeds, permeability now decreases sharply with growth in spite of the fact that temperatures are now higher (510° ± 20°C). The crystallization of the primary skarn most likely terminated near the peak of the metamorphic event. Conditions have changed gradually to $f_{S_2} \cong 10^{-5.5}$, $f_{O_2} \cong 10^{-25}$, and $f_{CO_2} \cong 10^{+1.2}$. Salinities have remained at high levels. Pyroxene in all cases analyzed increases in FeO and possibly Al_2O_3 while dropping in MgO and MnO. Garnet becomes more grossular-rich in sample II, but in sample I it takes a sudden increase in FeO near the edge with an accompanying drop in Al_2O_3. The differ-

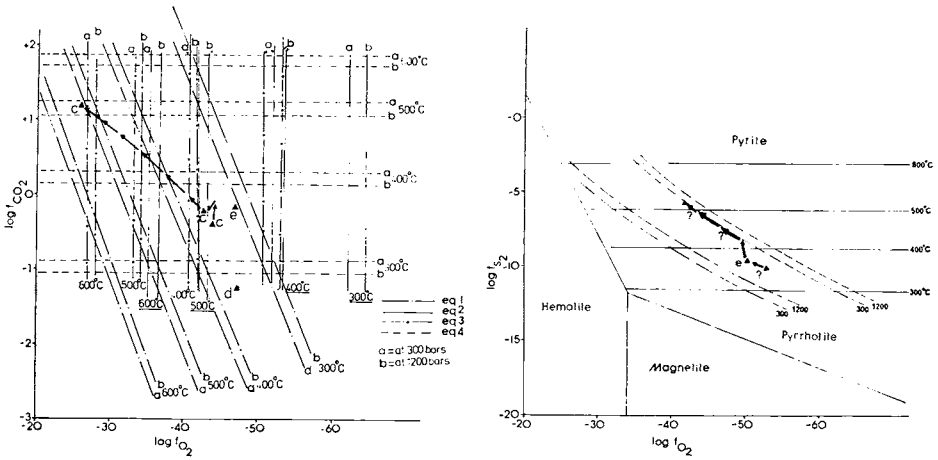

A. B.

Fig. 3. Interpreted conditions of formation of the King Island Scheelite deposit in log f_{CO_2}-log f_{O_2} and log f_{O_2}-log f_{S_2} space. The equations used are: (1) = $Ca_3Fe_2Si_3O_{12} + CO_2 + SiO_2 \rightleftarrows 2CaFeSi_2O_6 + CaCO_3 + 1/2\,O_2$, (2) = $CaWO_4 + S_2 + CO_2 \rightleftarrows WS_2 + CaCO_3 + 3/2\,O_2$, (3) $CaMoO_4 + S_2 + CO_2 \rightleftarrows MoS_2 + CaCO_2 + 3/2\,O_2$, (4) $CaCO_3 + SiO_2 \rightleftarrows CaSiO_3 + CO_2$, and (5) $FeS + 1/2\,S_2 \rightleftarrows FoS_2$. In (A) points "e" and "d" indicate the intersection of curves for eqs 1 and 2-3, and 2-3 and 4 respectively at 370°C. These points assume the garnet-derived temperature of 370°C is coincidental with the abrupt decrease of powellite in scheelite and the beginning of the pyrite overgrowth or reaction with pyrrhotite. The trend indicated by "c" is on the basis of the intersection of curves 1 and 4 and assumes conditions were on or near the quartz + calcite–wollastonite equilibrium curve. Point "c" in (A) is the same as "e" in (B). The trend in (B) assumes the conditions were near the pyrite–pyrrhotite equilibrium curve and, as such, is highly interpretive. The phase areas other than the pyrite–pyrrhotite ones in (B) are those for 300° after Helgeson (1969).

ence between the two samples is probably due to the marble-hornfels relations mentioned as will be discussed. Scheelite remains fairly constant in composition with only 0.2 to 1.0 wt percent powellite. The process is terminated while the hydrothermal fluid is still possibly supercritical. Conditions can alternate to produce quartz + calcite or wollastonite in this outer zone of the garnet, which is manifested by other concentric zones of wollastonite fibers occurring at different levels in the garnet, marking specific times of CO_2 release. The equilibria terminates in the quartz + calcite field.

8. Reactions between the hornfels and marble locally but away from the skarn have persisted evolving CO_2, H_2O, S_2, K^+, and Na^+ continuously. With the decrease permeabilities envisioned and metamorphic minerals perhaps healing the fractures previously developed (an observed phenomena in the skarn) the fugacities and activities of these volatile constituents increase to relatively high levels. These constituents react with the previously formed skarn minerals to produce the assemblage epidote–ferrohastingsite–quartz–calcite–pyrite. The degree of alteration depends very much on local conditions related to both the quantity of hornfels + marble reacted (see fig. 1, sample I and II; fig.

2) and the ease with which the volatiles can escape in different layers. The solution of CO_2 (and S, $SO^{4=}$, Ca^{++}, et cetera) into the 5 wt percent NaCl solutions would thus drop the critical point at 370°C significantly. Unfortunately, the experimental data in the entire system H_2O–CO_2–NaCl is insufficient to delineate exact values, but the data does suggest rather low pressures. No high-gas phase fluid inclusions were observed in the garnet near the wollastonite fibers; however, this is not an insurmountable problem. It is possible only one of the phases is trapped (for example, Roedder, 1967, p. 566), and fluid inclusions in the garnet are not abundant.

The statement that the pressure was equivalent to 1 to 2 km of rock (400-600 bars) is substantiated by the following evidence:

A. Lack of CO_2 liquid phase observed in any of the fluid inclusions. The formation of two liquids is greatly enhanced by moderate salinities but is, in part, a phenomenon of higher pressures (Takenouchi and Kennedy, 1965).

B. Two phase phenomena. If the hypothesis involving the two phase phenomena is sufficiently justified from the evidence presented, this delineates the pressure and temperature conditions. A solution of pure water with 5 wt percent dissolved NaCl boils at approx 450° and 350 bars total pressure (Sourirajan and Kennedy, 1962). A pure H_2O–CO_2 solution at its critical point at 370° gave a value of about 300 bars total pressure with a CO_2 content of about 10 mol percent (Takenouchi and Kennedy, 1964).

C. Crushing experiments on the fluid inclusions done at La Trobe and North Ryde yielded semiquantitative values of 450 to 500 bars for the temperatures suggested.

D. Low pressures seem most reasonable if calculations of the maximum possible stratigraphic thickness are done. Unfortunately, the outcrop in the general area is poor except along the coast, but thicknesses greater than 3 km are most unlikely with the probable depth being 1 to 2 km.

In addition, there is some evidence to support a model that fracturing and, presumably, pressure release is generally common in other skarn deposits. Price and Fenne (1972) describe scheelite grains from the Pine Creek District, Calif., where pure scheelite rims surround Mo-enriched scheelite cores which are fractured. The fractures are filled with rim-type scheelite, and the authors believe a period of fracturing preceded the deposition of the outer rim. It seems most probable that with increasing amounts of CO_2 evolved from the calc–silicate producing reactions, eventually pressure release by fracturing must occur with a subsequent change in the character of the products.

The moderate to high salinities observed in the fluid inclusions of the deposit can be explained in one of three ways, namely:

A. by a highly saline solution derived solely or largely from the magmatic source,

B. by a process of ultra filtration,

C. by boiling of dilute solutions, possibly involving a vapor pocket.

Explanation (A) in unlikely but still possible. Isotopic evidence usually suggests that hydrothermal oxygen and sulphur generally are of meteoric origin, but from a quantitative point of view, enough fluid could possibly be derived from the granodiorite to produce a significant amount of skarn. The deciding factor would be the concentration of W in the fluid phase. It is most likely too low, so that fluids besides the plutonic ones are necessary. Explanation (B) is clearly a possibility. Hanshaw and Cohen (1973) have convincingly shown both from experimental and field studies that shales can behave as semi-permeable membranes allowing uncharged species like H_2O through but retaining charged ions like Cl^- and Na^+. The only other requirement is a hydraulic head difference on both sides of the shale membrane. The method has been used to explain the extreme salinities observed in oil field brines (Bredehoeft and others, 1963; Hitchon, Billings, and Kloran, 1971), especially where no evaporite horizons exist to increase potentially the salinities to values beyond those of marine water. The process has not been tested at elevated temperatures and pressures but seems a distinctly possible method to produce high salinities at the King Island situation, because the beds dip toward the pluton, thus facilitating movement of surface water down dip or, more ideally, marine water, as well as there being many semi-permeable shale layers (now hornfels) which are continuous over long distances. Whether the process is operational when true micas such as biotite are present is not known, but the ultra filtration could occur up dip in particular strata outside the influence of the pluton. The process would best explain why small scale skarn interbeds between hornfels interbeds are of varying compositions. In some, a wollastonite zone occurs intermediate between the skarn and the marble, while in others this does not occur. The NaCl content of a solution very much affects the possible CO_2 content (Takenouchi and Kennedy, 1965) which, in turn, would very much affect whether calcite + quartz or wollastonite (+ CO_2) are stable. Clearly, at high salinities and low relative values of CO_2, wollastonite would be stable while at the same temperature and total pressure, but at lower salinities, quartz + calcite would be stable.

During the growth of the garnet described from sample II, a point was reached where salinity values increased and wollastonite was stable in preference to quartz + calcite. The reason quartz + calcite became stable later in the garnet's growth by this model would be due to a decrease in the efficiency of the ultra filtration process caused by the destruction of the phyllosilicates in the hornfels during increased metamorphism and possible flushing out of the high salinity water by more dilute fluids at the end of the garnet producing episode. Salinities at the edge of the garnet are still rather high, however. If this process were indeed present to a major degree, then the localization of the

skarn is dependent in part upon the orientation of the bedding, a potentially important ore control.

Explanation (C) is most reasonable, because it best explains the increase in salinity with the related fracturing and wollastonite crystallization in the garnet. The solution needs to reach its critical point, where the two phase area exists. The one fluid (vapor?) area would rise forming a vapor pocket up dip from the aqueous phase which may or may not reach the surface. Circulation of fluids in response to the heat anomaly (granite) would arrive at the stratigraphic position, where the conditions of the critical point occur. Here a NaCl rich aqueous fluid could occur with a CO_2–H_2O rich vapor phase. The vapor pocket could form rapidly during the fracturing period mentioned. Circulation of fluids due to the heat source supplied by the cooling pluton would attain the high salinity values or even increase them.

The reason the chemical zoning in garnet in samples I and II is different is problematical. Pyroxene in both cases shows a general increase in FeO with decreases in MgO, SiO_2, and MnO. The difference between the two samples may well be due to the amount of hornfels with its attendant mineral zonation already described. The accompanying study (Kwak, 1978) shows that the amount of Al_2O_3 to be removed from both systems is necessarily small. For a 10 cc volume exchange between each of the rock types in both specimens (1-2 mols per 10 cc of rock), these values are probably within analytical error. Presumably, the available Al^{+3} in sample I is depleted as the termination of garnet growth proceeds, and only significant amounts of Fe^{+3} are added. The grossularite present as a zone between the hornfels and marble in the case of both samples has persisted in spite of the reaction of the marble to skarn which occurred later. This grossularite could have behaved essentially as an Al_2O_3 sink for the marble–hornfels reactions. In the case of sample I, the previous grossularite zone appears to have been largely unaffected by the skarn producing episode, while in the case of sample II, only remnants of the once continuous grossularite garnet zone remain. The model must be invoked that although the supply of Al^{+3} to sample I skarn garnet was originally high (near 8 percent Al_2O_3 in the garnet) due to the most abundant hornfels bordering that skarn, with increasing growth the supply was largely exhausted, and conditions were not able to react with the remnant grossularite zone and supply Al^{+3} to the growing skarn garnet. In the case of sample II, the initial supply was low (near 2 wt percent Al_2O_3 in the garnet), but conditions changed so that the grossularite zone reacted with the skarn-forming fluid releasing necessary Al^{+3}. This is substantiated by the ragged grossular et cetera relicts in sample II but not in sample I. The differences could be due to the high salinities in the outer zone of sample II garnets and not, apparently, of sample I garnets.

The fluid inclusion data suggest the skarn minerals nucleated at low temperatures, until scheelite-producing skarn genesis stopped. This

suggests that the skarn was not produced by the advance of zones with complete crystallization away from the granite but rather as increasing temperature zones of partial crystallization advanced. Sample I would represent a skarn of nearly complete crystallization with the almost complete reaction of calcite (4.0 mol percent), whereas sample II is still not a completely crystallized layer (16.5 mol percent calcite). If zones of complete crystallization extend outward, permeability would most likely sharply decrease, and skarn crystallization would cease.

The identification of anhydrite in the fluid inclusions (pl. 2) is problematical because the solid phases, which originally crystallized from this fluid, contain sulphide not sulphate. To produce sulphate from sulphide involves the liberation of H^+ and, as some authors suggest, the loss of hydrogen out of the fluid inclusion by diffusion. Whether a model involving the loss of H^+ from the fluid inclusion is necessary depends on the quantities involved. If we take the following equilibria at 300°C (1 bar pressure) from Helgeson (1969)

$$S_2(g) + 2H_2O \rightleftarrows 2H_2S(aq) + O_2(g), \log K_{300} = -27.21 \qquad (A)$$

and

$$H_2S + 2O_2 \rightleftarrows SO_4^{=} + 2H^+ \qquad (B)$$

and if we use the values suggested for the fluids at 300°C as follows

$$S = 10^{-10} \text{ to } 10^{-12} \text{ mols}, O_2 = 10^{-30} \text{ to } 10^{-40}, H_2O = 1 \text{ mol } (a_{H_2O} \cong 1)$$

for eq (A) then the concentration of $H_2S(aq) \cong 10^{-4}$. This assumes activity = concentration which is reasonable at these concentrations. For every mol of $H_2S(aq)$, two mols of H^+ are produced (eq B) or 2×10^{-4} mols H^+. If we consider that neutrality of water at 300° is pH ≅ 5.5, then the effect of reducing sulphide to sulphate would be to change the pH of the fluid by only about one pH unit. The consequences of this are that a measurement of the pH of sulphate bearing fluid inclusions cannot be directly used.

ACKNOWLEDGMENTS

I wish to thank the personnel at the King Island Scheelite mine for allowing me access to the mine and for allowing me to sample the deposit. Mr. David Sewell and Mr. Angus Ferguson are thanked for their indispensible aid with the electron microprobe analyses done with the A.R.G.C. microprobe at the University of Melbourne. Mr. Peter Eadington of the C.S.I.R.O. Mineral Science Laboratory, North Ryde (N.S.W.) is thanked very kindly for the great amount of time he devoted to my attempts at fluid inclusion studies. Discussions with Professor Allan White and Dr. H. Wayne Nesbitt of this department contributed greatly to the geochemical interpretation and to correct my fuzzy thinking. Last, but not least, Mr. Lindsay Howe and Mrs. Helene English of this University are thanked for their help with the photography and typing respectively. The blame for any errors in the manuscript rest on my shoulders, however.

Appendix
Mineral analyses

	1	2	3	4	5	6	7	8	9	10
SiO_2	35.81	36.32	35.63	35.35	36.56	36.36	51.31	53.58	53.02	50.04
TiO_2	0.23	0.43	1.65	0.76	0.84	0.61	0.00	0.03	0.03	0.00
Al_2O_3	3.04	6.84	18.33	17.05	12.46	9.56	0.28	0.11	0.27	0.47
Fe_2O_3	27.26	21.70	8.01	7.59	14.94	18.24	-	-	-	-
FeO	-	-	-	-	-	-	19.58	9.72	3.93	13.48
MnO	1.10	0.49	0.19	0.33	0.27	0.96	1.53	1.19	0.63	1.99
MgO	0.04	0.03	5.75	7.15	0.06	0.27	4.41	11.41	16.23	9.30
CaO	32.25	32.64	28.33	29.90	34.74	34.27	22.96	25.16	25.46	25.02
Na_2O	0.00	0.04	0.02	0.06	0.00	0.06	0.14	0.11	0.05	0.17
K_2O	0.01	0.00	0.00	0.02	0.00	0.00	0.00	0.00	0.03	0.02
BaO	0.00	0.00	0.00	0.00	0.00	0.01	0.00	0.00	0.00	0.00
Cr_2O_3	0.04	0.03	0.00	0.08	0.02	0.00	0.04	0.04	0.00	0.00
NiO	0.01	0.00	0.03	0.02	0.00	0.00	0.00	0.03	0.00	0.00
WO_3	0.00	0.00	0.00	-	-	-	0.00	0.00	-	-
MoO_3	0.00	0.00	0.00	-	-	-	0.00	0.00	-	-
Cl	-	-	-	-	-	-	-	-	-	-
Total	99.79	98.92	97.91	98.22	100.29	100.34	100.25	101.38	99.65	100.59
Volatiles										
Si	5.980	5.967	5.590	5.582	5.791	5.851	Si 2.023	2.001	1.965	1.941
Al	0.020	0.023	0.410	0.418	0.209	0.147	Al -	-	0.035	0.021
	6.00	6.00	6.00	6.00	6.00	6.00	2.02	2.00	1.97	1.96
Ti	0.029	0.053	0.195	0.090	0.100	0.074	Ti -	0.001	0.008	-
Al	0.572	1.312	2.790	2.731	2.264	1.649	Al 0.013	0.005	-	-
Fe^{+3}	3.382	2.656	0.836	0.882	1.783	2.187	Fe^{+2} 0.648	0.304	0.122	0.432
Cr	0.005	0.003	-	0.011	0.001	0.000	Mn 0.051	0.038	0.020	0.065
Mn	0.155	0.124	0.025	0.044	0.036	0.131	Mg 0.539	0.633	0.896	0.538
Mg	0.010	0.007	1.344	1.663	0.014	0.065	Ca 0.970	1.007	1.011	1.040
Ca	5.751	5.746	4.769	5.066	5.896	5.911	Na 0.022	0.014	0.002	0.010
Na	-	-	0.004	0.008	-	0.005	K -	-	0.001	-
K	-	-	-	0.002	-	-	Cr 0.008	0.008	-	-
Ni	0.001	-	0.004	0.002	-	-	Ni -	0.003	-	-
	5.92	5.86	6.15	6.80	5.95	6.11	2.97	2.96	2.06	2.05

	11	12	13	14	15	16	17	18	19	20
SiO_2	51.65	50.04	50.02	0.10	0.00	0.00	0.00	0.00	30.70	53.93
TiO_2	0.01	0.00	0.09	0.00	0.04	0.00	0.00	0.05	36.89	0.00
Al_2O_3	0.27	0.47	0.43	0.00	0.00	0.02	0.05	0.03	1.54	3.34
Fe_2O_3	-	-	-	-	-	-	-	-	-	-
FeO	9.00	13.48	13.73	0.57	0.20	0.08	0.12	0.00	0.94	16.65
MnO	0.18	1.99	2.01	0.27	0.24	0.06	0.04	0.00	0.05	0.16
MgO	12.66	9.30	9.07	0.01	0.01	0.02	0.61	0.02	0.06	10.72
CaO	25.36	25.02	25.14	56.04	56.69	56.42	57.21	19.81	28.07	11.74
Na_2O	0.04	0.17	0.25	0.06	0.03	0.04	0.03	-	0.07	0.85
K_2O	0.00	0.02	0.00	0.03	0.02	0.00	0.02	-	0.08	0.04
BaO	0.00	0.00	0.00	0.00	0.00	0.00	0.05	0.02	0.00	0.02
Cr_2O_3	0.00	0.00	0.00	0.05	0.02	0.02	0.00	0.06	0.00	0.07
NiO	0.00	0.00	0.00	0.00	0.00	0.03	0.00	-	0.02	-
WO_3	-	-	-	-	-	-	-	77.40	-	-
MoO_3	-	-	-	-	-	-	-	1.40	-	-
Cl	-	-	-	-	-	-	-	-	-	-
Total	99.09	100.54	100.72	57.13	57.24	56.79	58.15	99.79	98.42	97.55
Volatiles				42.87	42.76	43.21	41.85			2.45
Si	1.967	1.941	1.940	Si 0.002	-	-	-	W 5.657	Si 4.073	Si 7.881
Al	0.012	0.021	0.045	Ti -	0.001	-	-	Mo 0.182	Al -	Al 0.119
	1.98	1.96	1.99	Al -	-	-	-	3.84	Ti 3.681	8.00
Ti	-	-	0.003	Fe^{+2} 0.016	0.009	0.003	0.003	Al 0.04	Al 0.239	Ti -
Al	-	-	-	Mn 0.007	0.002	0.002	0.002	Ti 0.001	Fe^{+2} 0.104	Al 0.693
Fe^{+2}	0.287	0.437	0.445	Mg 0.001	2.05 0.001	2.07 0.001	2.04 0.001	2.12 Ca 3.876	3.89 Mn 0.006	1.04 Fe^{+2} 2.035
Mn	0.006	0.065	0.066	Ca 2.023	2.048	2.032	2.083	Ba 0.001	Mg 0.012	Mn 0.020
Mg	0.719	0.538	0.524	Na 0.004	0.004	0.001	0.001	Cr 0.004	Ni 0.001	Mg 2.395
Ca	1.033	1.040	1.045	K	0.000	-	-			Ca 1.844
Na	0.003	0.010	0.005	Cr		0.001	-		Ca 3.991	Na 0.235
K	-	-	-	Ni		0.001	-		Na 0.018	4.02 K 0.007
Cr	-	-	-	C 1.973	1.963	1.980	1.939		K 0.014	Ba 0.001
Ni	-	-	-							Cr 0.008
	2.05	2.08	2.09							Ni -
										7.18

Appendix (cont.)

	21	22	23	24	25	26	27	28	29	30
SiO_2	41.47	41.78	51.13	50.12	37.57	37.51	35.19	57.54	36.99	Fe 47.09
TiO_2	0.98	1.05	0.00	0.04	2.40	2.09	2.52	0.00	0.29	Ni 0.10
Al_2O_3	10.48	10.37	0.02	0.01	13.52	13.65	13.31	19.70	17.50	Mn 0.54
Fe_2O_3	–	–	–	–	–	–	–	–	–	Co 0.00
FeO	18.86	17.66	0.16	0.27	4.47	4.72	4.42	0.78	23.44	Cu 0.25
MnO	0.34	0.34	0.38	0.07	0.23	0.19	0.28	0.02	0.15	S 52.01
MgO	9.64	10.15	0.20	0.11	2.73	2.67	2.79	0.30	9.85	
CaO	11.97	12.09	47.92	47.86	35.05	35.77	37.79	0.22	0.29	
Na_2O	1.86	1.91	0.01	0.01	0.00	0.02	0.00	11.91	2.86	
K_2O	1.45	1.51	0.02	0.01	0.01	0.00	0.01	0.11	3.35	
BaO	0.00	0.04	0.03	0.00	0.00	0.00	–	0.06	0.01	
Cr_2O_3	0.00	0.02	0.00	0.00	0.00	0.00	–	0.02	0.00	
NiO	0.02	0.01	0.00	0.00	0.00	0.00	–	–	–	
WO_3	–	–	–	–	–	–	–	–	–	
MoO_3	–	–	–	–	–	–	–	–	–	
Cl	–	–	–	–	0.10	0.17	0.18	–	–	
Total	97.24	96.99	99.87	98.47	96.17	96.79	96.53	100.66	94.79	
Volatiles					3.83	3.21	3.49	–		
Si	6.433	6.430	Si 1.982	1.978	Si 17.648	17.847	16.910	Si 11.816	Si 5.013	Fe 1.020
Al	1.567 8.00	1.570 7.97	Al 0.001	–	Al 0.202 18.00	0.151 18.00	1.090 18.00	Al 4.023	Al 2.187 8.00	Ni 0.002
								Fe^{+2} 0.114		Mn 0.010 1.04
Ti 0.114	0.122	Ti –	0.001	Ti 0.850	0.748	0.911		Mn 0.003	Ti 0.033	Co –
Al 0.344	0.312	Al –	–	Al 7.231	7.427	6.325		Mg 0.078	Al 0.966	Cu 0.004
Fe^{+2} 2.447	2.273	Fe^{+2} 0.005	0.009	Fe^{+2} 1.760 11.85	0.939 11.08	1.776 11.17			Fe^{+2} 2.974 4.22	
Mn 0.045	0.440	Mn –	0.002	Mg 1.917	1.893	1.998			Mg 2.228	S 1.961 1.96
Mg 2.223	2.328	Mg 0.011 2.00	0.006 2.04	Mn 0.092		0.114			Mn 0.019	
Ca 1.983 7.83	1.994 8.34	Ca 1.995	2.023						Ca 0.047	
Na 0.311	0.570	Na 0.002	0.002	Na –	0.003	–		Na 0.000	Na 0.035 1.532	
K 0.285	0.296	K 0.002	0.001	Ca 17.692 17.69	18.230 18.24	19.458 19.46		Ca 0.041	K 0.640	
Ba –	0.002	Ni –	–	K 0.003	–	0.006		K 0.025	Ba 0.001	
Cr –	0.001	Ba 0.002	–					Ba 0.004		
Ni 0.002	0.001			OH 6.024 6.18	5.048 5.25	5.700 5.80				
				Cl 0.153	0.199	0.145		Ab 98.4		
								An 1.0		
								Or 0.6		

	31	32	33	34	35	36	37	38	39	40	41	42
SiO_2	37.09	35.45	35.26	34.86	48.70	48.96	48.70	49.89	0.05	0.00	0.00	0.00
TiO_2	0.43	0.22	0.08	0.79	0.05	0.02	0.20	0.03	0.01	0.01	0.02	0.01
Al_2O_3	12.40	4.91	2.12	2.96	0.28	0.18	0.23	0.15	0.00	0.01	0.00	0.01
Fe_2O_3	14.63	24.15	22.79	24.87	–	–	–	–		–	–	–
FeO	–	–	–	0.43	27.47	25.13	25.51	24.94	0.46	0.41	0.13	0.06
MnO	1.63	0.49	0.35	0.23	1.20	1.87	1.94	2.37	0.25	0.48	0.11	0.03
MgO	0.05	0.03	0.03	34.23	0.52	1.88	0.41	1.31	0.02	0.01	0.02	0.01
CaO	34.97	35.16	34.16	0.01	23.49	23.16	22.38	22.91	56.28	56.27	57.12	57.56
Na_2O	0.01	0.01	0.00	0.02	0.08	0.04	0.04	0.04	0.02	0.04	0.01	0.04
K_2O	0.01	0.02	0.00	0.02	0.01	0.00	0.00	0.00	0.00	0.02	0.00	0.02
BaO	0.14	0.00	0.05	0.03	0.01	0.01	0.03	0.00	0.00	0.00	0.00	0.00
Cr_2O_3	0.01	0.00	0.00	0.00	0.00	0.05	0.03	0.00	0.03	0.00	0.01	0.00
NiO	0.00	0.00	0.00	0.00	0.03	0.01	0.00	0.05	0.00	0.01	0.00	0.01
WO_3	–	–	–	–	–	–	0.00	0.00				
MoO_3	–	–	–	–	–	–	0.00	0.00				
Cl	–	–	–	–	–	–	–					
Total	100.39	100.48	99.78	100.42	101.84	101.33	99.29	100.65	57.15	57.26	57.42	57.75
Volatiles									42.85	42.73	42.58	42.25
Si	5.812	5.850	5.932	5.815	Si 1.977 1.99	1.978 1.99	2.008 2.01	2.049 2.05	Si 0.001	–	–	
Al	0.188 6.00	0.150 7.00	0.068 6.00	0.185 6.00	Al 0.013	0.008	–	–	Fe 0.015	0.003	0.002	0.001
									Mn 0.008	0.013	0.003	
Ti 0.051	0.027	0.010	0.099	Ti 0.002	0.001	0.001	0.001	Mg 0.009	2.04	0.000 1.03	0.001	2.02 1.95
Al 2.371 3.93	0.800 3.83	0.348 3.83	0.393 3.84	Al –	–	0.011	0.007	Ca 2.034		1.017	1.032	1.044
Fe^{+3} 1.705	2.969	3.483	3.339	Fe^{+2} 0.190	0.854	0.898	0.822	Na 0.001		0.002	–	0.002
				Mn 0.001	0.004	0.008	0.006	K –		0.001	–	
Mn 0.215	0.059	0.050	0.041	Mg 0.008	0.133	0.005	0.040					
Mg 0.012	0.007	0.007	0.057	Ca 1.022 2.04	1.002 2.02	0.998 1.98	1.000 1.96	C 1.971	1.97	0.984 1.98	0.980 1.98	0.977 1.98
Ca 5.872	6.217 6.32	6.147	6.118 6.25	Na 0.006	0.005	0.001	0.003					
Na – 8.11	0.019	– 6.21	0.006	K 0.001	–	–	–					
K –	0.008	–	0.008	Ba –	–	0.001	–					
Ba 0.059		0.003		Cr –	0.003	0.001	–					
				Ni 0.001	–	–	0.002					

APPENDIX (cont.)

	43	44	45	46	47	48	49	50	51
SiO_2	0.13	0.22	37.60	37.39	42.65	29.96	49.84	Co 0.00	0.00
TiO_2	0.06	0.04	0.10	0.45	0.25	34.35	0.00	Ni 0.12	0.12
Al_2O_3	0.01	0.05	25.54	24.38	6.49	1.99	0.17	Mn 0.58	0.53
Fe_2O_3	-	-	10.74	11.19	-	-	-	Cu 0.23	0.24
FeO	0.08	0.11	-	-	32.49	1.17	2.11	Fe 60.35	47.83
MnO	0.00	0.00	0.22	0.14	0.86	0.13	0.72	S 36.85	52.22
MgO	0.05	0.04	0.00	0.00	0.60	0.00	0.00		
CaO	19.11	18.80	23.11	23.66	12.27	29.93	46.80		
Na_2O	-		0.01	0.00	0.43	0.01	0.00		
K_2O	-		0.00	0.00	0.83	0.02	0.00		
BaO	0.03	0.12	0.04	0.00	0.00	0.00	0.00		
Cr_2O_3	0.02	0.00	0.00	0.01	0.04	0.01	0.00		
NiO	-		0.00	0.00	-	-	0.00		
WO_3	81.62	67.60	0.00	0.00	0.00	0.00	-		
MoO_3	0.14	16.24	0.00	0.00	0.00	0.00	-		
Cl		-	-	-	-	-	-		
Total	101.25	103.22	97.38	97.22	96.82	98.58	99.64	98.13	100.94
Volatiles									
W	3.999	2.864	Si 2.874	2.870	Si 7.003	Si 4.040	Si 1.969	Co -	-
Mo	0.011	1.216	Al 0.126	0.130	Al 0.997	Al -	Al 0.012	Ni 0.002	0.002
	4.01	4.08	3.00	3.00	8.00	4.04	1.98	Mn 0.009	0.010
Si	0.025	0.039	Ti 0.006	0.013	Ti 0.030	Ti 3.483	Al -	Ca 0.003	0.003
Ti	0.008	0.005	Al 2.152	2.076	Al 0.262	Al 0.313	Fe^{+2} 0.029	Fe 0.951	1.027
Al	0.002	0.007	Fe^{+3} 0.618	0.646	Fe^{+2} 4.462	Fe^{+2} 0.132	Ca 1.985		
Fe^{+2}	0.013	0.017	Mg -	-	Mn 0.119	Mn 0.015			
Mg	0.003	0.011	Mn 0.018	0.009	Mg 0.147	Mg -			
Ca	3.873	3.620	Ca 1.847	1.946	Cr 0.002				
Ba	0.001	0.008	Ba -	-	Ca 2.159	Ca 4.324			
Cr	0.001		Na 0.001	-	Na 0.136	Na -			
	3.93	3.71	2.79	2.74	K 0.174	K 0.000			
			1.95	1.95	5.02	3.94	2.01		
			1.85		2.47	4.33			

Sample I:

1. Edge of garnet in garnet skarn, 2. Center of garnet in garnet skarn, 3. Garnet in wollastonite rock, 4. Garnet in marble, 5. Garnet in garnet zone at marble-hornfels contact, 6. Garnet at pyroxene rock-garnet skarn contact, 7. Edge of pyroxene in garnet skarn near analyzed garnet, 8. Center of pyroxene in garnet skarn near analyzed garnet, 9. Pyroxene in wollastonite rock, 10. Pyroxene in marble, 11. Pyroxene in pyroxene zone at marble-hornfels contact, 12. Pyroxene near garnet zone at pyroxene rock-garnet skarn contact, 13. Pyroxene well within (2 cm) pyroxene rock, 14. Calcite in garnet skarn near analyzed garnet, 15. Calcite in coarse grained calcite zone between wollastonite rock and garnet skarn, 16. Calcite in wollastonite zone, 17. Calcite in marble, 18. Scheelite in hornfels, 19. Sphene in hornfels, 20. Amphibole in hornfels, 21. Edge of amphibole in amphibole hornfels, 22. Center of amphibole in amphibole hornfels, 23. Wollastonite in wollastonite rock, 24. Wollastonite in wollastonite zone at the marble-hornfels contact, 25. Edge of vesuvianite in wollastonite rock, 26. Center of vesuvianite in wollastonite rock, 27. Vesuvianite in vesuvianite zone at marble-hornfels contact, 28. Plagioclase in hornfels, 29. Biotite in hornfels, 30. Pyrite in garnet skarn. 31. Edge of garnet, garnet skarn; 32. Composition of garnet where wollastonite fibers occur, 33. Center of garnet, garnet skarn, 34. Remnant of garnet, amphibole skarn, 35. Edge of pyroxene, garnet skarn, 36. Center of pyroxene, garnet skarn, 37. Edge of pyroxene, amphibole skarn, 38. Center of pyroxene, amphibole skarn, 39. Calcite, garnet skarn, 40. Calcite, amphibolite skarn, 41. Calcite, coarse grained calcite zone at amphibole skarn-marble boundary, 42. Calcite, marble, 43. Edge of scheelite, garnet skarn, 44. Center of scheelite, garnet skarn, 45. Edge of epidote, amphibole skarn, 46. Center of epidote, amphibole skarn, 47. Amphibole, amphibole skarn, 48. Sphene, amphibole skarn, 49. Wollastonite fibers in garnet, garnet skarn, 50. Pyrrhotite core, garnet skarn, 51. Pyrite rim, garnet skarn.

The garnets modal proportions are on the basis of 24 oxygen atoms; pyroxene, 6; wollastonite, 6; calcite, 6; scheelite, 17; sphene, 20; amphibolite, 23; vesuvianite, 72; epidote, 12; biotite, 22; plagioclase, 32; and pyrite, 2 sulphur atoms.

REFERENCES

Bartholmé, P., and Dimanche, F., 1967, On the Paragenesis of Ilvaite: Soc. géol. Belgique Bull. 90, p. 533-558.

Bredehoeft, J. D., Blyth, G. R., White, W. A., and Maxey, G. B., 1963, Possible mechanism for the concentration of brines in subsurface formations: Am. Assoc. Petroleum Geologists Bull. 47, p. 257-269.

Brock, K. J., 1972, Genesis of Garnet Hill skarn, Calaveras County, California: Geol. Soc. America Bull., v. 83, p. 3391-3404.

Buseck, P. R., 1966, Contact metasomatism and ore deposition, Concepcion Del Oro Mexico: Econ. Geology, v. 61, p. 97-136.

Deer, W. A., Howie, R. A., and Zussman, J., 1966, An introduction to the rock-forming minerals: London, Longmans, 528 p.

Edwards, A. B., Barker, G., and Callow, G. J., 1956, Metamorphism and metasomatism at King Island scheelite mine: Geol. Soc. Australia Jour., v. 3, p. 55-90.

Govorov, I. N., and Filippova, T. G., 1968, Geochemical types of ore-bearing hydrothermal solutions: Proc. of Coffi, v. 1, p. 47.

Greenwood, H. J., 1967, Wollastonite: Stability in H_2O–CO_2 mixtures and occurrence in a contact metamorphic aureole near Salmo, B.C., Canada: Am. Mineralogist, v. 52, p. 1669-1681.

Gustafson, W. I., 1974, The stability of andradite, hedenbergite and related minerals in the system Ca–Fe–Si–O–H: Jour. Petrology, v. 15, p. 455-496.

Hanshaw, B. B., and Cohen, T. B., 1973, Ultrafiltration by a compact clay membrane II sodium ion exclusion at various ionic strengths: Geochim. et Cosmochim. Acta, v. 37, p. 2311-2327.

Helgeson, H. C., 1969, Thermodynamics of hydrothermal systems at elevated temperatures and pressures: Am. Jour. Sci., v. 267, p. 729-804.

Helgeson, H. C., Brown, T. H., and Leeper, R. H., 1969, Handbook of theoretical activity diagrams depicting chemical equilibria in geologic systems involving an aqueous phase at one atmosphere and 0° to 300°C: San Francisco, Freeman Cooper and Co., 241 p.

Hitchon, B., Billings, G. K., and Klovan, J. E., 1971, Geochemistry and origin of formation of waters in the Western Canada sedimentary basin III factors controlling chemical composition: Geochim. et Cosmochim. Acta, v. 35, p. 567-598.

Huchenholz, H. G., and Yoder, H. S., 1971, Andradite stability relations in the $CaSiO_3$–Fe_2O_3 join up to 30 kb: Neues Jahrb. Mineralogie, v. 114, p. 246-280.

Hsu, L. C., and Gulli, P. E., 1973, Origin of the scheelite–powellite series of minerals: Econ. Geology, v. 68, p. 681-696.

Kelley, K. K., 1960, Contributions to the data on Theoretical Metallurgy XIII High temperature heat-content, Heat capacity and Entropy data for the Elements and Inorganic compounds: U.S. Bur. Mines Bull. 584, 232 p.

Kennedy, G. C., 1954, Pressure-volume-temperature relations in CO_2 at elevated temperatures and pressures: Am. Jour. Sci., v. 252, p. 194-225.

Kissling, A. L., and Pomîrleanu, V., 1970, On the formation temperature of minerals from the Ocna de Fier-Dognecea skarn, Roumania [abs.], *in* Collected Abstracts, IMA-IAGOD Meetings: Tokyo, Science Council of Japan, p. 275.

Korobeynikov, A. F., 1968, Physico-chemical processes of gold mineralization of the Kommuner ore field: Proc. of Coffi, v. 2, p. 44.

Kwak, T. A. P., 1978, Mass balance relationships and skarn-forming processes at the King Island Scheelite Deposit, King Island, Tasmania, Australia: Am. Jour. Sci., v. 278, p. 943-968.

Large, R. R., 1972, Metasomatism and scheelite mineralization at Bold Head, King Island: Australian Inst. Mining Metallurgy Proc., no. 238, p. 31-45.

Mamontov, B. V., 1968, Temperature conditions of formation of the South-Yangikan Copper-Molybdenum Deposit: Proc. of Coffi, v. 1, p. 57.

Mason, P. K., Frost, M. T., and Read, S. J. B., 1969, Computer programs for calculating corrections in quantitative X-ray micro-analysis: Natl. Phys. Lab., U.K. Div. Inorganic and Metallic Structure, Rept. No. 2.

Morgan, B. A., 1975, Mineralogy and Origin of skarns in the Mount Morrison Pendant, Sierra Nevada, California: Am. Jour. Sci., v. 275, p. 119-142.

Nye, P. B., and Knight, C. L., 1953, The King Island Scheelite Mine: Australia Commonwealth Dept. Supply and Shipping, Mineral Resources Survey Bull. 11.

Pitcher, W. S., 1950, Calc–silicate skarn veins in the limestone of Lough Anure, Co. Donegal: Mineralog. Mag., v. 29, p. 126-141.

Price, W. H., and Fenne, F. K., 1972, Microprobe study of molybdenum distribution in scheelites from the Pine Creek Mine, Bishop District, California: Geol. Soc. America Abs. with Program, v. 4, p. 220.

Robie, R. A., and Waldbaum, D. R., 1967, Thermodynamic properties of minerals and related substances at 298.15°K (25.0°C) and one atmosphere (1.013 bars) pressure and at higher temperatures: U.S. Geol. Survey. Bull. 1259, 256 p.

Roedder, Edwin, 1963, Studies of fluid inclusions II: Freezing data and their interpretation: Econ. Geology, v. 58, p. 167-211.

———— 1967, Fluid Inclusions as samples of ore fluids *in* Barnes, H. L., ed., Geochemistry of Hydrothermal Ore Deposits: New York, Holt, Rinehart and Winston, p. 515-574.

Scharbert, H. G., 1966, Andradit Führende Einschaltungen im Marmor von Hartenstern (Kl. Kremstal, N.O.): Neues Jahrb. Mineralogie Mh, p. 221-223.

Schearer, J. A., ms, 1973, The thermochemistry of garnets and some related compounds: Ph.D. thesis, Univ. of Chicago.

Shoji, T., 1975, Role of temperature and CO_2 pressure in the formation of skarn and its bearing on mineralization: Econ. Geology, v. 70, p. 739-749.

Sigurdson, D. R., and Lawrence, E. F., 1976, Mineral paragenesis and fluid inclusion thermometry at four tungsten deposits in the Western U.S.A.: Internat. Geol. Cong., 25th, Sydney, Australia, 1976, p. 813-814.

Sourirajan, S., and Kennedy, G. C., 1962, The system H_2O–NaCl at elevated temperatures and pressures: Am. Jour. Sci., v. 260, p. 115-141.

Takenouchi, S., and Kennedy, G. C., 1964, The binary system H_2O–CO_2 at high temperatures and pressures: Am. Jour. Sci., v. 262, p. 1055-1074.

———— 1965, The solubility of carbon dioxide in NaCl solutions at high temperatures and pressures: Am. Jour. Sci., v. 263, p. 445-454.

Tilley, C. E., 1951, The zoned contact skarn of the Broadford Area, Skye: Mineralog. Mag., v. 29, p. 621-666.

Toulmin, Priestly, III, and Barton, P. B., Jr., 1964, A thermodynamic study of pyrite and pyrrhotite: Geochim. et Cosmochim. Acta, v. 28, p. 641-671.